International Journal of Nanomedicine

Dovepress
open access to scientific and medical research

Open Access Full Text Article

ORIGINAL RESEARCH

Thermosensitive Betulinic Acid-Loaded Magnetoliposomes: A Promising Antitumor Potential for Highly Aggressive Human Breast Adenocarcinoma Cells Under Hyperthermic Conditions

This article was published in the following Dove Press journal:
International Journal of Nanomedicine

Claudia Geanina Farcas[1,2,*]
Cristina Dehelean[2,*]
Iulia Andreea Pinzaru[2]
Marius Mioc[2]
Vlad Socoliuc[3,4]
Elena-Alina Moaca[2]
Stefana Avram[2]
Roxana Ghiulai[2]
Dorina Coricovac[2]
Ioana Pavel[5]
Praveen Kumar Alla[5]
Octavian Marius Cretu[6]
Codruta Soica[2]
Felicia Loghin[1]

[1]Faculty of Pharmacy, Department of Toxicology, "Iuliu Haţieganu" University of Medicine and Pharmacy Cluj Napoca, Cluj Napoca, Romania; [2]Faculty of Pharmacy, "Victor Babeş" University of Medicine and Pharmacy Timisoara, Timisoara, Romania; [3]Laboratory of Magnetic Fluids, Center for Fundamental and Advanced Technical Research, Romanian Academy – Timisoara Branch, Timisoara, Romania; [4]Research Center for Complex Fluids Systems Engineering, Politehnica University of Timisoara, Timisoara, Romania; [5]Department of Chemistry, Wright State University, Dayton, OH, USA; [6]Faculty of Medicine, "Victor Babeş" University of Medicine and Pharmacy Timisoara, Timisoara, Romania

*These authors contributed equally to this work

Correspondence: Iulia Andreea Pinzaru; Marius Mioc
Email iuliapinzaru@umft.ro; marius.mioc@umft.ro

Purpose: Breast cancer presents one of the highest rates of prevalence around the world. Despite this, the current breast cancer therapy is characterized by significant side effects and high risk of recurrence. The present work aimed to develop a new therapeutic strategy that may improve the current breast cancer therapy by developing a heat-sensitive liposomal nano-platform suitable to incorporate both anti-tumor betulinic acid (BA) compound and magnetic iron nanoparticles (MIONPs), in order to address both remote drug release and hyperthermia-inducing features. To address the above-mentioned biomedical purposes, the nanocarrier must possess specific features such as specific phase transition temperature, diameter below 200 nm, superparamagnetic properties and heating capacity. Moreover, the anti-tumor activity of the developed nanocarrier should significantly affect human breast adenocarcinoma cells.

Methods: BA-loaded magnetoliposomes and corresponding controls (BA-free liposomes and liposomes containing no magnetic payload) were obtained through the thin-layer hydration method. The quality and stability of the multifunctional platforms were physico-chemically analysed by the means of RAMAN, scanning electron microscopy-EDAX, dynamic light scattering, zeta potential and DSC analysis. Besides this, the magnetic characterization of magnetoliposomes was performed in terms of superparamagnetic behaviour and heating capacity. The biological profile of the platforms and controls was screened through multiple in vitro methods, such as MTT, LDH and scratch assays, together with immunofluorescence staining. In addition, CAM assay was performed in order to assess a possible anti-angiogenic activity induced by the test samples.

Results: The physico-chemical analysis revealed that BA-loaded magnetoliposomes present suitable characteristics for the purpose of this study, showing biocompatible phase transition temperature, a diameter of 198 nm, superparamagnetic features and heating capacity. In vitro results showed that hyperthermia induces enhanced anti-tumor activity when breast adenocarcinoma MDA-MB-231 cells were exposed to BA-loaded magnetoliposomes, while a low cytotoxic rate was exhibited by the non-tumorigenic breast epithelial MCF 10A cells. Moreover, the in ovo angiogenesis assay endorsed the efficacy of this multifunctional platform as a good strategy for breast cancer therapy, under hyperthermal conditions. Regarding the possible mechanism of action of this multifunctional nano-platform, the immunocytochemistry of the MCF7 and MDA-MB-231 breast carcinoma cells revealed a microtubule assembly modulatory activity, under hyperthermal conditions.

Conclusion: Collectively, these findings indicate that BA-loaded magnetoliposomes, under hyperthermal conditions, might serve as a promising strategy for breast adenocarcinoma treatment.

Keywords: magnetoliposomes, hyperthermia, betulinic acid, breast adenocarcinoma

submit your manuscript | www.dovepress.com
DovePress
http://doi.org/10.2147/IJN.S269630

Introduction

Worldwide, breast carcinoma is the most commonly diagnosed malignancy that affects women, with over one million new patients each year.[1,2] According to the World Health Organization (WHO),[3] the incidence rate varies significantly across the world, ranging from 19.3/100 000 women in Eastern Africa to 89.7/100 000 women in Western Europe. Nevertheless, the survival rate depends a lot on the stage of carcinoma detection; thus, women in developed countries such as North America, Japan and Sweden present a survival rate of 80%, while women in low-income countries have a survival rate of 40%. Therapeutic approach of breast carcinomas is defined by the molecular expression of estrogen receptor (ER), progesterone receptor (PR), human epidermal growth factor receptor 2 (HER2), and the Ki-67 cellular proliferation marker. Thus, for ER-positive tumors the hormone therapy is usually implemented. However, the most aggressive subtype of breast cancer – the triple-negative breast cancer (TNBC) does not express ER, PR or HER2 and is characterized by a poor prognosis, a high rate of relapse, and ineffective therapy. Furthermore, it is commonly associated with women under 50 years old.[2,4,5] In this case, for high-grade carcinomas, the treatment is associated with the administration of anthracyclines (doxorubicin and epirubicin) and taxanes (paclitaxel and docetaxel) among other chemotherapeutics.[6] Although doxorubicin is considered to be the most active and widely used substance in the treatment of breast cancer,[7] in addition to its side effects, the mechanism of resistance (by inducing changes in topoisomerase II expression) is another huge limitation for its use in breast adenocarcinoma therapy.[6] Therefore, the development of a new therapeutic strategy for TNBC treatment could help overcome key therapeutic challenges such as the side effects and chemotherapy resistance presented by conventional treatment. To address this limitation, the current study approaches a new therapeutic strategy for inducing cytotoxicity of human adenocarcinoma cells by developing a nano-based formulation suitable to incorporate a potent anti-tumor agent that manifests minimal cytotoxic effect on healthy cells and also to be able to address a hyperthermic approach of the carcinoma cells. Inducing hyperthermia in breast carcinomas presents a series of advantages as the normal cells surrounding the tumor tissue exhibit a higher resistance to temperatures around 43–46 °C, while tumor cells are known to be significantly affected by hyperthermia treatment, up to 46 °C[8–12.] Nevertheless, hyperthermia treatment success is based on biocompatible temperatures, up to 46 °C,[8–11] exceeding this temperature will induce necrosis of both normal and tumor cells.[13] In recent years, magnetic nanoparticles (MNPs) have been developed and gained significant attention in drug delivery, hyperthermia approach, and remote-controlled drug release[10,12,14–17.] Among them, magnetic iron oxide nanoparticles (MIONPs) are the most commonly used due to their biocompatibility, good colloidal stability (if a suitable capping agent is used), and high magnetization potential.[18–20]

The anti-tumor agent chosen in the present study is betulinic acid – BA, a pentacyclic triterpene declared as one of the most promising anti-tumor agents in a screening supported by the United States National Cancer Institute (NCI).[21] It has been assumed that BA induces apoptosis via an intrinsic pathway, which affects mitochondrial membrane integrity and thereby bypasses the classical chemotherapy resistance[22,23], thus providing an important advantage for patients that develop resistance to the regular chemotherapeutics, such as doxorubicin.[6] However, the hydrophobic structure of BA and the relatively short half-life in the systemic circulation limit its bioavailability. Therefore, the development of an adequate drug delivery system that can overcome these limitations is essential to improve its pharmacokinetics properties.[24,25]

In this regard, liposomes are considered ideal nanostructures for entrapping both hydrophobic drugs in their lipid bilayer structure and hydrophilic MNPs in their aqueous core.[12,26] Liposomes entrapping MNPs are generically entitled magnetoliposomes.[17,26] These nano-based structures are among the most successfully utilized biocompatible, biodegradable, and non-immunogenic drug carriers, as they are designed similarly to the cell membrane in order to bypass solubility issues, in vivo toxicity, and poor stability manifested by other carrier systems.[27–31]

Magnetoliposomes possess the advantage of remote drug release when applying an external magnetic field, taking advantage of the hyperthermia-inducing features expressed by the MNPs that could control the phase transition of magnetoliposomes from the gel to the liquid state.[17]

Based on these aspects, the main goal of this work was to develop a novel multifunctional platform with both hyperthermia-inducing and remote drug delivery features able to release its payload (BA and MIONPs) under controlled hyperthermic conditions, thus overcoming the

above-mentioned therapeutic challenges associated with the use of BA.

In the current study, the nano-based BA-loaded magnetoliposomal system was found to induce an enhanced cytotoxic effect on MDA-MB-231 cells, under hyperthermic conditions, as compared to BA alone, whereas the non-tumorigenic breast cell line – MCF 10A manifested a slightly diminished viability. The anti-tumor effect of the developed platform is related to both BA and MIONPs activity; BA promotes significant microtubule alterations, whereas MIONPs content is responsible for a specific nuclear alteration, called enucleation. It was also found that the anti-tumor effect of the multifunctional platform is correlated with the impairment of the angiogenesis process.

Materials and Methods

Reagents

Cholesterol, L-α-phosphatidylcholine (lecithin), 1.2-distearoyl-sn-glycerol-3-phosphoethanolamine– N-[amino (polyethylene glycol)-2000] (DSPE-PEG2000), and betulinic acid were purchased from Sigma-Aldrich Chemie GmbH (Taufkirchen, Germany). Methanol was obtained from Merck (Darmstadt, Germany), ammonium formate from Agilent (Santa Clara, CA, USA), and ultrapure deionized water was provided by a Milli-Q® Integral Water Purification System from Merck Millipore (Darmstadt, Germany). All reagents were of analytical grade purity, commercially available. Specific cell culture media, high glucose Dulbecco's Modified Eagle's Medium (DMEM), Eagle's Minimum Essential Medium (EMEM) and Dulbecco's Modified Eagle's Medium and Ham's F12 medium (1:1 mixture) with L-Glutamine and HEPES (DMEM:F12) were purchased from ATCC (American Type Culture Collection). Fetal calf serum (heat-inactivated FCS), antibiotic mixture, Trypsin EDTA and Trypan blue reagent were purchased from Sigma-Aldrich Chemie GmbH (Taufkirchen, Germany). Epidermal Growth Factor (EGF) and phosphate buffer saline (PBS) were obtained from Thermo Fisher Scientific (Massachusetts, USA).

Cell Lines

The cell lines used in the present study, MDA-MB-231 (ATCC® HTB-26), MCF7 (ATCC® HTB-22), and MCF 10A (ATCC® CRL-10,317) were acquired from ATCC (Manassas, VA, United States) as frozen vials and stored in liquid nitrogen, at −196 °C.

Magnetic Iron Oxide Nanoparticles Coated with Citric Acid (MIONPs*CA) Synthesis

Magnetic iron oxides nanoparticles (MIONPs) were synthesized following the combustion method as described in detail by Ianos et al, using iron nitrate nonahydrate ($Fe(NO_3)_3$•$9H_2O$) and a double amount of fuel – citric acid monohydrated ($C_6H_8O_7$•H_2O). Briefly, reagents were mixed and dissolved in distilled water, quickly heated to 400 °C in a heating mantle with a design to trigger the ignition of the combustion reaction. After several minutes the obtained reaction product was hand grinded, washed (fresh distilled water) and dried.[32] The physico-chemical analysis of the MIONPs revealed the presence of two types of iron oxide: magnetite nanoparticles (Fe_3O_4) and maghemite nanoparticles (γ-Fe_2O_3), with spherical shape and an average hydrodynamic diameter of 76 nm. Further, MIONPs were moistened for 2 days in a mixture formed of distilled water and 96% ethanol, afterwards sonicated for several hours and covered with citric acid (CA) monolayer, in a basic environment. The MIONPs coated with CA were dispersed in distilled water, leading to a stable colloidal suspension with high zeta potential (around −47 mV).

Magnetoliposomes Synthesis

The magnetoliposomes were prepared through the well-described thin-layer hydration method.[30,33] Briefly, L-α-phosphatidylcholine:cholesterol:DSPE-PEG2000:BA (100mg:12.5mg:10mg:10mg) were dissolved in a 1:1 (v/v), methanol:chloroform solvent mixture and stirred until a clear solution was obtained. The solvent mixture was then removed using a rotary evaporator and the resulting lipid film was hydrated with an aqueous magnetic suspension, corresponding to 10 mg of MIONPs (total lipid: MIONPs molar ratio of 4:1). The mixture was left to hydrate for 24 h before redispersion through sonication for 30 min in a Qsonica Q700 Sonicator. Un-encapsulated magnetic nanoparticles were removed by magnetic decantation, separated through centrifugation at 0.86 RCF and the resulting solution was extruded through a 0.2-μm membrane and stored at 4 °C until further use. Empty/blank nano-liposomes (without MIONPs and betulinic acid) were prepared similarly and used as controls. A graphical representation of the BA-loaded magnetoliposomes is shown in Figure 1.

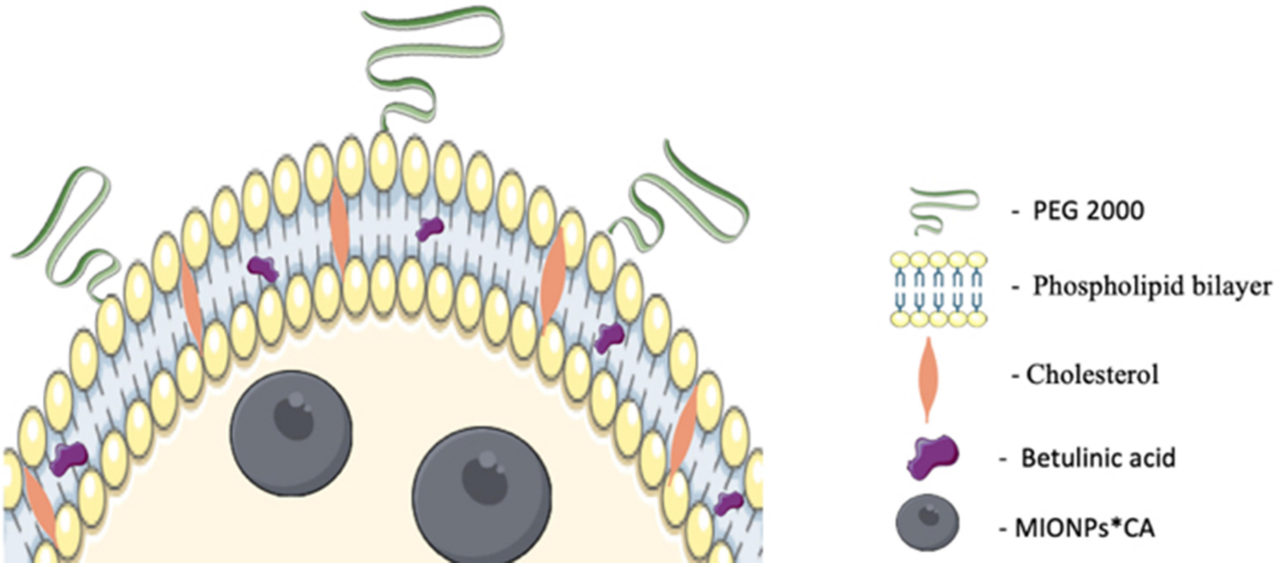

Figure 1 Graphical representation of a BA-loaded magnetoliposome. MIONPs*CA are incorporated in the aqueous core, while BA is entrapped in the lipid bilayer of the liposome. (Image realized by applying Servier Medical ART illustration: http://smart.servier.com).

Raman Spectroscopy Characterization of BA-Loaded Magnetoliposomes

Micro-Raman spectra of BA-loaded magnetoliposomes and controls were collected in the 100–4000 cm^{-1} spectral region using a LabRam HR-800 system (Horiba Jobin Yvon, Inc.). Samples were excited with a HeNe laser of 632.8 nm (15 mW output) through a confocal Raman BX41 microscope (100x Olympus objective) and the following parameters were employed in the acquisition of the inelastic backscattering signals: a holographic grating of 600 grooves mm^{-1}, a confocal hole of 300 μm, a thermoelectrically cooled Andor CCD camera of 1024 × 256 pixels, neutral filters of optical densities of 0.3–4, acquisition times of 5, 15, and 30 s, and five cycles for each sample. Under these experimental conditions, the spectral resolution was about 1 cm^{-1}. The spectra were collected using the LabSpec v.5 software and were processed in Origin 8.6 software.

Morphology and Elemental Composition

The morphology and ultrastructure of BA-loaded magnetoliposomes (Lip+MIONPs*CA+BA) was determined by scanning electron microscopy (SEM) and the elemental composition was confirmed by energy dispersive X-ray analysis (EDAX). SEM-EDAX analysis was performed with EDX detection on a scanning electron microscope (SEM), using an EDAX detector (ZAF Quantification—Standardless, Element Normalized) with FEI Quanta 250 microscope (Eindhoven, Holland).

DLS and ζ-Potential Measurements

The hydrodynamic diameter and the surface charge of the liposomal samples were determined using a dynamic light scattering (DLS) instrument (Malvern Zatasizer Nano ZS) at 37 °C. The stock solutions of liposomal samples and MIONPs*CA colloidal suspensions were diluted 3 times and 10 times, respectively, with Milli Q water.

Magnetic Characterization

Magnetometry

The mass magnetization curves at room temperature (22 °C) of the magnetic MIONPs and of the magnetoliposomes (Lip+MIONPs*CA, Lip+MIONPs*CA+BA) were measured by the means of an ADE Technologies VSM 880 instrument. Using the MIONPs and magnetoliposomes saturation magnetization (M_{sat}) values, the MIONPs mass percentage (%m MIONPs) in the magnetoliposomes was calculated according to the following formula:

$$\%\text{mMIONPs} = \frac{\text{Msat magnetoliposomes}}{\text{Msat MIONPs}} \text{x}100\% \quad (1)$$

Magnetically Induced Heat Generation

The heating ability of the magnetic MIONPs in AC high-frequency magnetic fields was investigated using an in-house built equipment. The AC magnetic field with 98kHz

frequency and 10 kA/m field was generated using a commercial induction heater. The sample was contained in a polyethylene plastic cylindrical flask thermally insulated with polystyrene foam. The sample temperature was measured using an Optocon FOTEMP1-OEM optical fiber thermometer. The data acquisition was made using a National Instruments virtual instrument. The Intrinsic Loss Power (ILP)[34] of the MIONPs was determined using the stepped heating method.[35]

Thermal Analysis

The heating behavior of the BA-loaded magnetoliposome (Lip+MIONPs*CA+BA) was studied within the range of 25–80 °C by thermal analysis, using a Netzsch 449 C instrument. The thermogravimetric (TG) and differential scanning calorimetry (DSC) curves were recorded using aluminum crucibles, under a nitrogen flow of 20 mL/min, at a heating rate of 5 °C/min.

Evaluation of Fe and BA Encapsulation Efficiency

Determination of Fe Concentration

Fe content of the magnetoliposome stock solutions (Lip+MIONPs*CA and Lip+MIONPs*CA+BA) was determined via a colorimetric assay, which involved the formation of a Fe^{3+}–sulfocyanate complex.[36] The absorbance of the resulting complex was measured at 480 nm using a T70 UV/VIS spectrophotometer (PG Instruments Ltd.) and the final concentration of Fe was calculated using a linear, external calibration curve obtained from standard solutions, with Fe concentrations ranging from 650 $\mu g \cdot mL^{-1}$ to 7.4 $mg \cdot mL^{-1}$. Encapsulation efficiency (EE) was determined by applying the following formula:

$$EE\% = \frac{Fe_{in\ liposomes}}{Fe_{total}} x100\% \quad (2)$$

[37]

Determination of BA Concentration

The amount of BA not incorporated in the liposomes was determined based on the fact that lipid interference can occur. A 6120 LC-MS analytical system from Agilent (Santa Clara, CA, USA) which consisted of a 1260 Infinity HPLC coupled with a Quadrupolar (Q) mass spectrometer equipped with an electrospray ionization source (ESI) was utilized. The OpenLAB CDS ChemStation Workstation software was employed to control the instrument, acquire and process the LC-MS data. Samples were analyzed on a Zorbax Eclipse Plus C18 column (3.0 mm x100 mm x 3.5 µm) at 40 °C. The mobile phase was 85% methanol and 15% 1 mM of ammonium formate in isocratic elution, at a flow rate of 1 $mL \cdot min^{-1}$. UV detection was achieved at λ= 200 nm and BA was identified at 2.82 min retention time. Mass spectrometric detection was accomplished by ESI ionization and SIM detection in the negative ion mode [$M\text{-}H^+$] at m/z = 455.3. An external calibration curve was obtained by a 7-point plot in the 50–2000 $ng \cdot mL^{-1}$ range ($R^2 > 0.999$ linearity) and was used for the sample quantification.

The encapsulation efficiency (EE) and the drug loading capacity (DLC) were estimated using the following formulas:

$$EE\% = \frac{BA_{total} - BA_{free}}{BA_{total}} x100\% \quad (3)$$

[38]

$$DLC\% = \frac{BA_{encapsulated}}{totallipids} x100\% \quad (4)$$

[37]

Cell Culture

Two distinct breast adenocarcinoma cell lines and a non-tumorigenic control cell line were utilized for the in vitro evaluation of the BA-loaded magnetoliposomes. The following tumorigenic cell types were selected due to their different genotypes: MDA-MB-231, a triple-negative human breast adenocarcinoma cell line, and MCF7 cells, a hormone-dependent cell line that is progesterone and estrogen receptor-positive with a high Ki-67 expression.[39] The non-tumorigenic cells were MCF 10A-breast epithelial cells. All cells were maintained under standard conditions: a humidified atmosphere of 5% CO_2, at 37 °C, in a Steri-Cycle i160 incubator (Thermo Fisher Scientific, USA). Cells were cultured as monolayers in specific growth media. MDA-MB-231 cells and MCF7 cells were maintained in DMEM and EMEM, respectively, supplemented with 10% FCS and 0.1 $mg \cdot mL^{-1}$ streptomycin, and 100IU mL^{-1} penicillin. MCF 10A cells were cultured in DMEM:F12 medium supplemented with 20 $ng \cdot mL^{-1}$ epidermal growth factor (EGF), 0.01 $ng \cdot mL^{-1}$ insulin, 500 $ng \cdot mL^{-1}$ hydrocortisone, 5% FCS, and antibiotic mixture of 0.1 $mg \cdot mL^{-1}$ streptomycin, 100IU mL^{-1} penicillin. The medium was replaced every 2 days.

Treatment Protocol

Cells (MDA-MB-231, MCF7, and MCF 10A) were seeded in 6-, 12-, and 96-well culture plates according to the experimental needs and incubated until a confluent cell monolayer was reached. Cells were then exposed to final concentrations of 5 and 25 μM of BA that correspond to 5.94 and 29.71 $\mu g \cdot mL^{-1}$ of MIONPs. All experiments were performed under normothermic and hyperthermic conditions. The equivalent concentration of BA dissolved in DMSO was also tested and served as positive control. The cells were exposed to a maximum concentration of 0.5% DMSO, which was deemed non-toxic for in vitro applications.[40]

Hyperthermia Protocol

To simulate also the cytotoxic effects induced by test compounds under hyperthermic conditions, each experiment was carried in hyperthermia (43 °C). The hyperthermia protocol was performed as described by Kossatz et al, by incubating the cells at 43 °C for 90 cumulative equivalent minutes (CEM43).[41] A temperature treatment that is equivalent to an incubation time of 30 min at 46 °C.[9] When the hyperthermia period ended, the microplates were maintained under normal conditions until a total of 24 h incubation was achieved.

Cell Viability Assessment

In a primary screening, the effect of all test compounds on the viability rate of both adenocarcinoma cell lines (MDA-MB-231 and MCF7) and one mammary epithelial cell line (MCF 10A) was evaluated using the 3–4,5-dimethylthiazol-2-yl-2,5-diphenyltetrazolium bromide (MTT) assay. In brief, MCF7, MDA-MB-231, and MCF 10A cells were seeded onto 96-well plates at an initial density of $1x10^4$ cells/well. Next day, the medium was replaced with a fresh one containing the test compounds and cells were incubated for 24 h under normothermic and hyperthermic conditions. Afterward, 10 μL of MTT reagent was added in each well and the culture plates were incubated for 3 h. The mitochondrial reductase of the viable cells converted the yellow MTT to a dark, insoluble formazan salt. The formed crystals were dissolved by the addition of 100 μL of lysis buffer per well. Finally, the absorbance of the generated colour was spectrophotometrically analysed at 570 nm using a microplate reader (xMark™ Microplate Spectrophotometer, Bio-Rad Laboratories, Inc., Hercules, CA, USA). The experiments were performed in triplicate, with three wells for each concentration. The cell viability percentage was calculated according to the following formula:

$$\text{Viability}(\%) = \frac{\begin{array}{c}\text{Abs}_{\text{TS}} \pm \text{HT}_{\text{(with cells)}} \\ -\text{Abs}_{\text{TS}} \pm \text{HT}_{\text{(without cells)}}\end{array}}{\begin{array}{c}\text{Abs}_{\text{CNT(with cells)}} \\ -\text{Abs}_{\text{CNT(without cells)}}\end{array}} \text{x}100\% \quad (5)$$

where:

Abs $_{TS}$ = Absorbance of test sample

Abs $_{C\ NT}$ = Absorbance of control in normothermia

HT = hyperthermia

Cytotoxicity Assay

A cytotoxicity test that quantifies the amount of LDH (cytosolic enzyme) released into the media was performed similarly to the MTT assay. The extracellular leakage of this cytosolic enzyme is an indicator of the cytotoxic potential and the results can be further quantified by spectrophotometric analysis.[42,43] After incubating the cells for 24 h with the test compounds under normothermic and hyperthermic conditions, 50 μL/well of media containing the LDH released was transferred into a new plate and after that 50 μL reaction mixture was added in each well and mixed carefully. The plate was then incubated at room temperature, in the dark, for 30 min before adding 50 μL/well of stop solution. The absorbance was measured at 490 nm and 680 nm with a microplate reader (xMark™ Microplate Spectrophotometer, Bio-Rad Laboratories, Inc., Hercules, CA, USA)

In vitro Scratch Assay – Wound Healing Technique

The scratch assay test was employed to assess cell to cell interaction along with cell migration and proliferation potential. This technique is based on the formation of a cell-free area by scratching the cell monolayer along the well diameter with a sterile pipette tip. The cell growth in the scratched area is then supervised by taking pictures at certain time intervals.[44,45]

The three cell types were cultured to a density of 2.0×10^5 cells/well into 12-well plates until the optimal confluence was reached. Afterwards, a straight gap was drawn inside each well and the cellular debris were washed with 1x PBS. The scratched areas were treated with test samples and the plates were maintained under normothermic and hyperthermic conditions. Pictures were taken initially (normothermic conditions) and 24 h post-stimulation (normothermic and hyperthermic conditions) with an inverted microscope

(Olympus IX73, Tokyo, Japan) equipped with an integrated DP74 camera (Olympus, Tokyo, Japan). The scratched widths were determined with the calibrated scale measurement function of the camera software (CellSense Dimension) in order to quantify the migration rate. The following formula was applied:[46]

$$\text{Scratch closure after 24h}(\%) = \frac{Scratch\ surface(0h) - Scratch\ surface(24h)}{Scratch\ surface(0h)} \text{x}100\% \quad (6)$$

Fluorescence Immunocytochemistry

Cells were cultured on coverslips in 6-well plates (35 mm diameter) overnight and were then exposed to the test compounds for 24 h. After the incubation period ended, the cells were washed twice with ice-cold 1x PBS and fixed with 4% PFA in PBS for 30 min at room temperature. Thereafter, cells were washed again with 1x PBS, permeabilized with 2% Triton X-100/1x PBS, blocked with 30% FCS in 0.01% Triton X-100, and incubated with the primary antibody (α-tubulin antibody, Invitrogen by Thermo Fisher Scientific) in a dark humidity chamber, at 4 °C, overnight. The following day, cells were washed twice with 0.01% Triton X-100/1x PBS and incubated with fluorescent-labeled (Alexa Flour™ 488, Invitrogen by Thermo Fisher Scientific) goat anti-rabbit secondary antibody, in a dark humidity chamber, at 4 °C, for 1 h. After rinsing the cells five times with 0.01% Triton X-100/1x PBS, cell nuclei were counterstained with DAPI (4′,6′-diamidino-2-phenylindole) for 15 min. Finally, the coverslips were mounted on glass slides with Fluoromont™ aqueous mounting medium (Sigma-Aldrich, Munich, Germany) and observed under an Olympus IX73 microscope equipped with ultraviolet and blue excitation filters and DP74 camera (Olympus, Tokyo, Japan). Post-captured images were merged and adjusted for brightness and colour balanced using Image J software.

In ovo Angiogenesis Assessment Through Chick Chorioallantoic Membrane (CAM) Assay

The CAM assay is a simple alternative method to in vivo mouse models that offers the ability to assess the angiogenesis process.[47] The angiogenesis process is the phenomenon through which new blood vessels are emerging from the pre-developed vasculature.[48] This process is known to have a significant impact on tumor growth and proliferation. Evaluation of test samples can be performed during specific embryonic days of development (EDD), between EDD 7–10, when the chick embryo CAM shows specific characteristics of the tumor angiogenesis process.[49] Thus, this method is widely used in cancer research as a preliminary assay to murine experimental models.[47]

The method employed for the CAM assay was conducted as previously described.[43] Briefly, fertilized eggs (Gallus gallus domesticus) were sprayed with 70% alcohol to ensure the disinfection of the eggshell and afterwards the eggs were horizontally incubated in a controlled humidified atmosphere at 37 °C. On the 3rd EDD, approximately 5 mL of albumen was aspired through a small perforation in the pointed end of the eggshell. The following day, a window was cut on the upper side of the egg, that was further sealed to assure the physiologic conditions offered by the eggshell, and specimens were further incubated until the day of the experiment. To induce hyperthermic conditions the liposomal samples at the final concentration of 25 μM were maintained for 30 min at 46 °C in a water bath (Precision GP20, ThermoFisher Scientific) and 10 μL were immediately applied on the top of the CAM, inside the plastic ring that has been previously placed on the vascularized surface of the CAM. The liposomal samples were daily applied and the angiogenesis process was monitored between the 7th to 11th EDD by means of a stereomicroscope (Discovery 8 Stereomicroscope, Zeiss). Representative images were taken for further analysis using the Axio CAM 105 color, Zeiss digital camera and processed by Zeiss ZEN software and ImageJ software. The EDD 7 was considered the starting point of the experiment (0 h).

Angiogenesis inhibition (AI) could be quantified by morphometric analysis of daily recorded macroscopic images.[43] In this regard, the blood vessels (BV) that intersected the inoculation ring were determined and the following formula was applied:

$$\text{AI}(\%) = 1 - \frac{NoBV_{test\ sample}}{NoBV_{control}} \text{x}100\% \quad (7)$$

Statistical Analysis

The GraphPad Prism 8.3.0 software (GraphPad Software, San Diego, CA, USA) was used for the performance and presentation of the data. One-way ANOVA analysis was applied to determine the statistical differences followed by Tukey's post-test (* $p < 0.05$, ** $p < 0.01$, and *** $p < 0.001$, **** $p < 0.0001$ vs hyperthermia control cells). The results

were expressed as the mean ± standard deviation (SD) of three independent experiments (n=3).

Results

Physico-Chemical Characterization of BA-Loaded Magnetoliposome and Controls

The physico-chemical analysis of the magnetoliposomes was conducted by means of Raman spectroscopy, SEM-EDAX analysis.

Raman Analysis

The micro-Raman spectra of BA-loaded magnetoliposomes and corresponding active substrates, betulinic acid and MIONPs, are shown in Figure 2. Raman vibrational modes for the new BA-loaded magnetoliposomes were detected at 332, 395, 471, 560, 660, 995, 1059, 1349, 1457, 1600, 1865, 2091, 2647, 2897, and 3144 cm^{-1}. A careful analysis of the control samples (MIONPs NPs coated with citric acid, and BA alone) in conjunction with the current Raman literature[50–56] facilitated the identification of the Raman bands of BA-loaded magnetoliposomes and demonstrated their structural composition. The broad peaks at 995 and 1059 cm^{-1} of very strong relative intensity (Figure 2C) are indicators of the entrapment of BA in the lipid bilayer and the PEG functionalization of the magnetoliposomes, respectively. Other standalone BA marker bands at 463, 1348 and 1457 cm^{-1} in Figure 2A were observed at 471, 1349 and 1456 cm^{-1} in the Raman spectrum of BA-loaded magnetoliposomes (Figure 2C). A PEG characteristic peak (at 2890 cm^{-1}) was detected at 2897 cm^{-1} in the Raman spectrum of BA-loaded magnetoliposomes (Figure 2C).

Morphological Structure and Elemental Analysis

Morphological analysis was conducted by scanning electron microscopy (SEM) which showed relatively smooth-surfaced, agglomerated nanoparticles with a mean diameter below 200 nm (Figure 3); the freeze-dried cake appearance of BA-loaded magnetoliposomes does not undergo significant alterations. However, some irregularities can be noticed, as a consequence of the HV (high vacuum) set-up employed for this technique, described in the literature as a factor that influences the microscopic evaluation of lyophilized products.[57]

The chemical species utilized in the synthesis of BA-loaded magnetoliposomes were identified through EDAX analysis. As presented in Figure 3, only C, O, P, K and Fe were recorded within BA-loaded magnetoliposomes sample. The results were expressed in weight percent (Wt %) and atomic percent (At %) within Table S1.

Stability, Size, Magnetization, Heating and Thermal Analysis

Physical stability of the liposomal structures was assessed by taking pictures at different time points, for almost 1 month. The liposomal samples were stored at 4 °C and the colloidal suspension of MIONPs*CA was maintained at room temperature. All samples presented a good stability for 28 days and homogeneous appearance: neither small aggregation nor flocculation of the liposomal structures was observed. MIONPs*CA colloidal suspension showed no instability signs for more than 6 months (Figure S1).

Moreover, the measurement of the ζ-potential of each sample indicated a high stability of the liposomal structures against aggregation: Lip, Lip+MIONPs*CA, Lip +BA and Lip+MIONPs*CA+BA developed a ζ-potential of −21.6 mV, −29.4 mV, −28.0 mV and −19.7 mV, respectively (Table 1). In terms of mean diameter, all liposomal samples showed diameters below 200 nm, as follows: 177.6 nm for Lip, 153 nm for Lip+MIONPs*CA, 108.7 nm for Lip+BA, and 198.1 nm for Lip+MIONPs*CA+BA (Figure 4A).

The MIONPs used to obtain the magnetoliposomes, showed superparamagnetic behaviour with negligible coercivity and manifested a saturation magnetization of 48.7 emu/g (Figure 4B). The magnetometry indicated that magnetoliposomes (Lip+MIONPs*CA, Lip +MIONPs*CA+BA) possess superparamagnetic properties of 0.094 and 0.089 emu/g, respectively. The MIONPs mass percentage from both magnetoliposomes (Lip +MIONPs*CA, Lip+MIONPs*CA+BA) was determined by applying equation (1) which indicated the following values: 0.193%m and 0.183%m, respectively. The saturation magnetization of BA-loaded magnetoliposomes (Lip +MIONPs*CA+BA) is lower than that of the BA-free magnetoliposomes (Lip+MIONPs*CA), probably due to the additional BA mass. The heating capacity of MIONPs was determined by the Intrinsic Loss Power (ILP) analysis, which revealed a value of 0.178±0.032 $nH*m^2/kg$. Thus, by using ILP of MIONPs and the mass

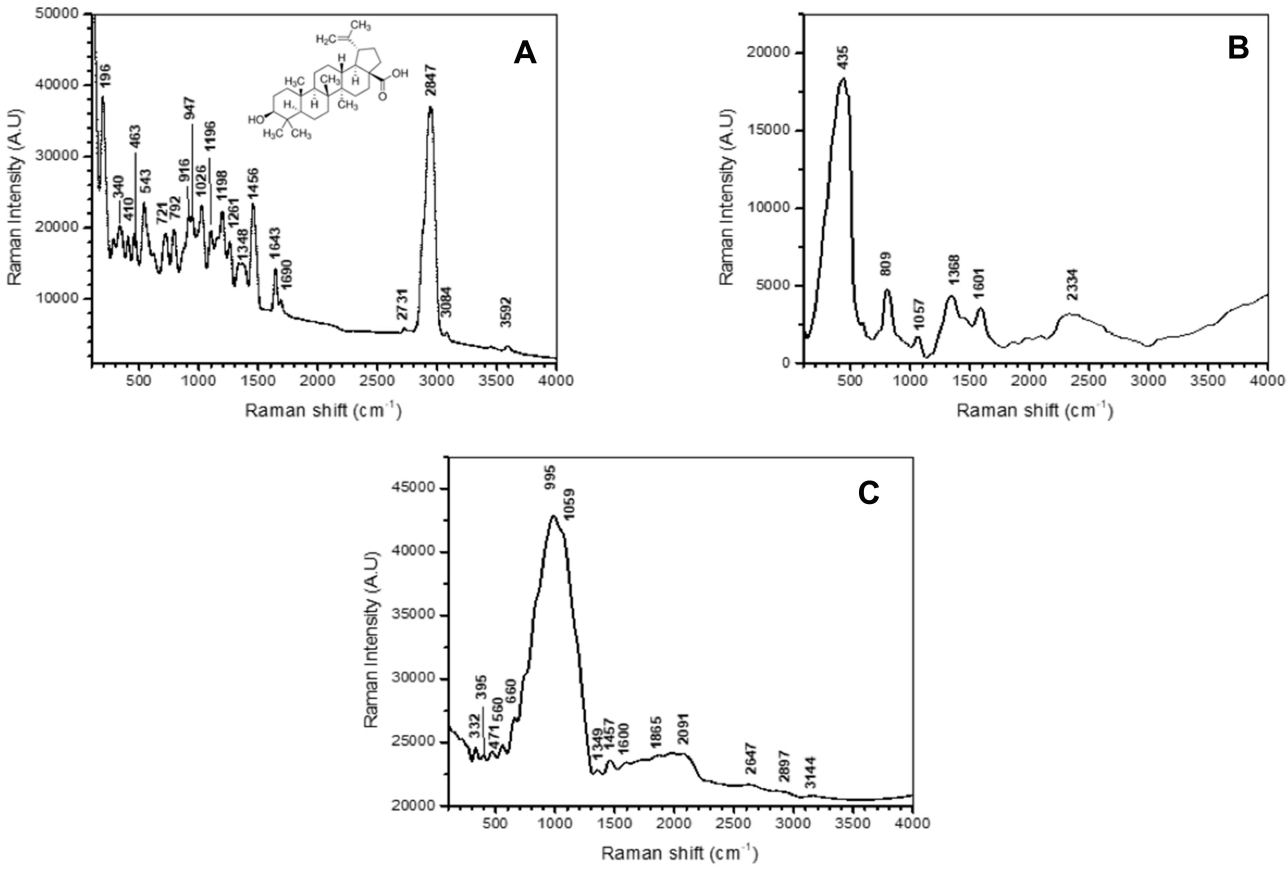

Figure 2 (**A**) Molecular structure and Micro-Raman spectra of betulinic acid (BA); (**B**) Micro-Raman spectra of magnetic iron oxide nanoparticles (MIONPs); (**C**) Micro-Raman spectra of BA-loaded magnetoliposomes.

percentage of magnetic loading, the ILP of magnetoliposomes can be estimated for the perspective of their use in magnetic hyperthermia experiments.

Thermal analysis of BA-loaded magnetoliposomes (Figure 4C) indicated an endothermic process at 45.9 °C, which is attributed to the transition of the phospholipid bilayer of the liposome from the gel to the liquid phase;[37] the process was accomplished without mass loss, as recorded on the TG curve.

Betulinic Acid and MIONPs*CA Encapsulation Within Liposomes

The total amount of free BA determined by LC-MS was 973 µg; thus, after applying equations (3) and (4), the encapsulation efficiency and drug loading capacity of BA within liposomes were determined to be 80.54% and 7.1%, respectively. The encapsulation efficiency of MIONPs*CA within BA-loaded magnetoliposomes calculated with equation (2) indicated an encapsulation efficiency of MIONPs*CA of 79.16%.

Cell Viability Assessment by MTT Assay

The MTT data sets of both human adenocarcinoma cell lines (MDA-MB-231 and MCF7) and one non-tumorigenic breast epithelial cell line (MCF 10A) are presented in Figure 5. MDA-MB-231 control cells were more sensitive to hyperthermia treatment, displaying a viability rate of approximately 70%, whereas MCF7 control cells expressed a higher viability percentage, around 85%. The most resistant cells to hyperthermia treatment were the MCF 10A cells, showing 90% viability. Lower MDA-MB-231 cell viability was recorded under hyperthermic conditions when the liposomal structures containing BA (Lip+BA and Lip+MIONPs*CA+BA) were compared with the active compound alone. The most significant reduction of the MDA-MB-231 viability was noticed when Lip +MIONPs*CA+BA sample was applied under hyperthermic conditions. In this case, the cells expressed the viability of 47.31% (vs 56.89% viability displayed by the MDA-MB-231 cells treated with BA alone, under hyperthermia).

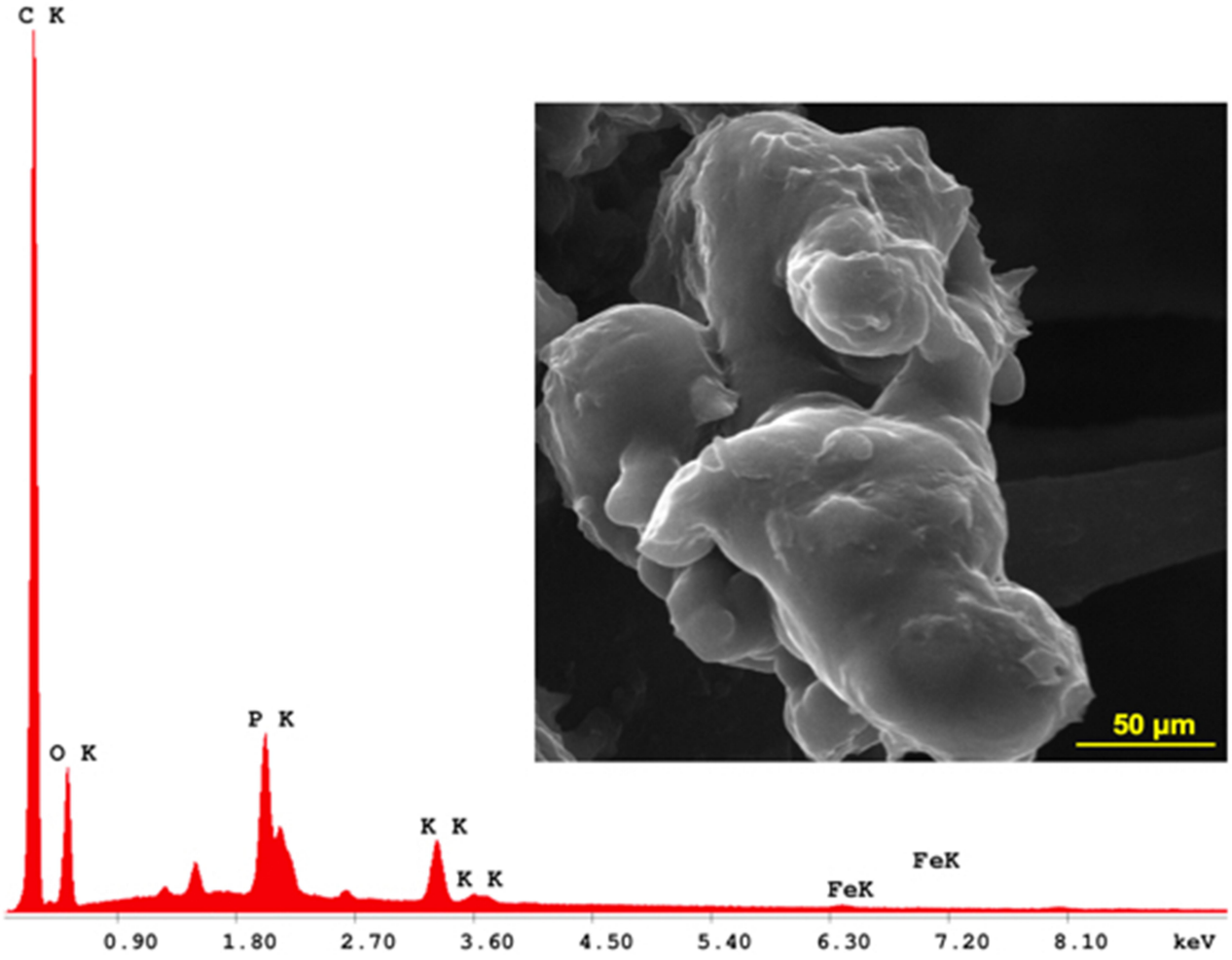

Figure 3 SEM-EDAX analysis of BA-loaded magnetoliposomes.

MCF7 cells responded quite different if compared to the MDA-MB-231 cells, the higher concentration (25 µM) induced cytotoxic effects rather independent of the thermal conditions applied. Thereby, it could be stated that the hyperthermic treatment significantly augmented MDA-MB-231 cell viability reduction after stimulation with Lip+MIONPs*CA+BA nanoformulations, while MCF7 cells were more resistant to this treatment.

Nevertheless, the viability of MCF 10A cells did not fall below 80% when exposed to liposomal samples, regardless of the thermal conditions applied.

The MTT assay emphasized the selective cytotoxic role played by BA-loaded platforms in human breast cell lines, causing a significant cytotoxic effect on the highly aggressive MDA-MB-231 cells and low viability inhibition (20%) of the non-tumorigenic breast MCF 10A cells.

Table 1 Physico-Chemical Characteristics of BA-Loaded Magnetoliposomes and Controls

Sample	DLS		ζ-Potential		Msat [emu/g]	%m MIONPs [%]
	Z-Average [nm]	PDI	ζ-Pot [mV]	ζ-Pot StdDev [mV]		
Lip	177.6	0.182	−21.6	−2.1	-	-
Lip+MIONPs*CA	153.0	0.218	−29.4	−2.8	0.094	0.193
Lip+BA	108.7	0.238	−28.0	−2.7	-	-
Lip+MIONPs*CA+BA	198.1	0.416	−19.7	−1.9	0.089	0.183

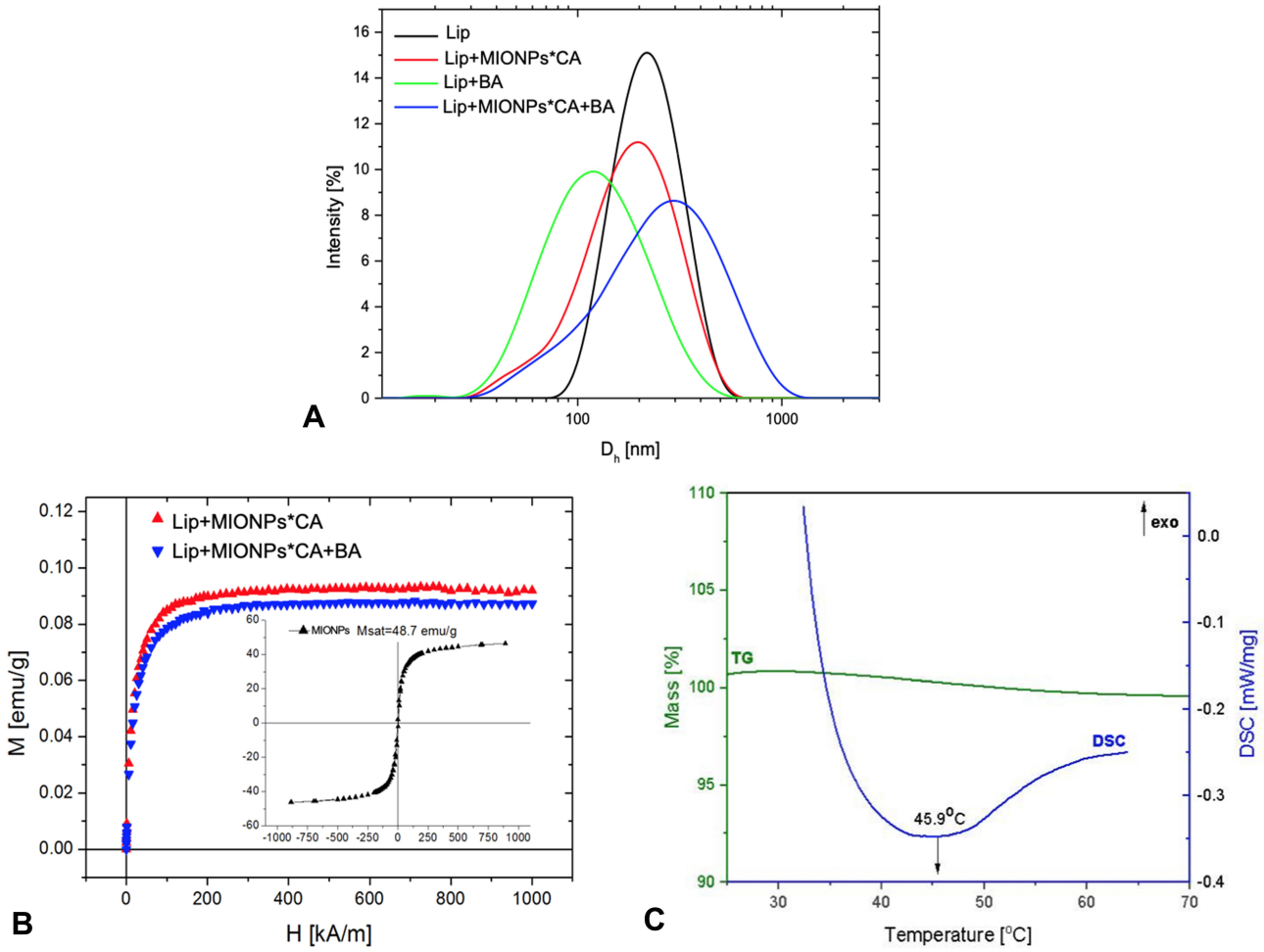

Figure 4 Graphical representation of: (**A**) intensity distribution of particles size of the liposomal samples; (**B**) magnetization curves of magnetoliposomes and control (MIONPs); (**C**) TG/DSC curves of BA-loaded magnetoliposome.

Cytotoxic Potential Assessment by the Means of Lactate Dehydrogenase (LDH) Release

The reduction in the cell viability observed through MTT test was further assessed by the means of LDH cytotoxicity assay; results are displayed in Figure 6.

Taking into account that this particular method present limitations in detecting low percentages of LDH, especially for short incubation periods (24 h) or processes affecting the intracellular activity of the cells,[58,59] this assay was performed only for the highest concentration, 25 μM, where the MTT test revealed a more significant cell viability decrease.

As shown in Figure 6, a moderate increase in the cytotoxic effect was induced by BA-free liposomal structures under hyperthermic conditions, compared to the results obtained under normothermic conditions, especially for the MDA-MB-231 cells. The cytotoxic rates displayed by MCF7 cells stimulated with test samples presented slight differences between normothermic and hyperthermic conditions, with the highest cytotoxic rate (7.50%) recorded after Lip+MIONPs*CA+BA treatment, under normothermic conditions. However, it could be observed that BA-loaded platforms induced a less cytotoxic effect and BA itself did not induce LDH released, which can be explained by the mechanism of action of BA.

MCF 10A cells showed no significant increase in the cytotoxic rate after treatment with liposomal samples under hyperthermic conditions. Nevertheless, MCF-10A cells treated with BA manifested the same effect as the tumorigenic cell lines exposed to BA, displaying no LDH released.

Cell Migration Assessment – a Wound Healing Technique

Cell migration assessment was conducted by means of the wound healing technique (Figure 7). It could be noticed that under normothermic conditions the MDA-MB-231

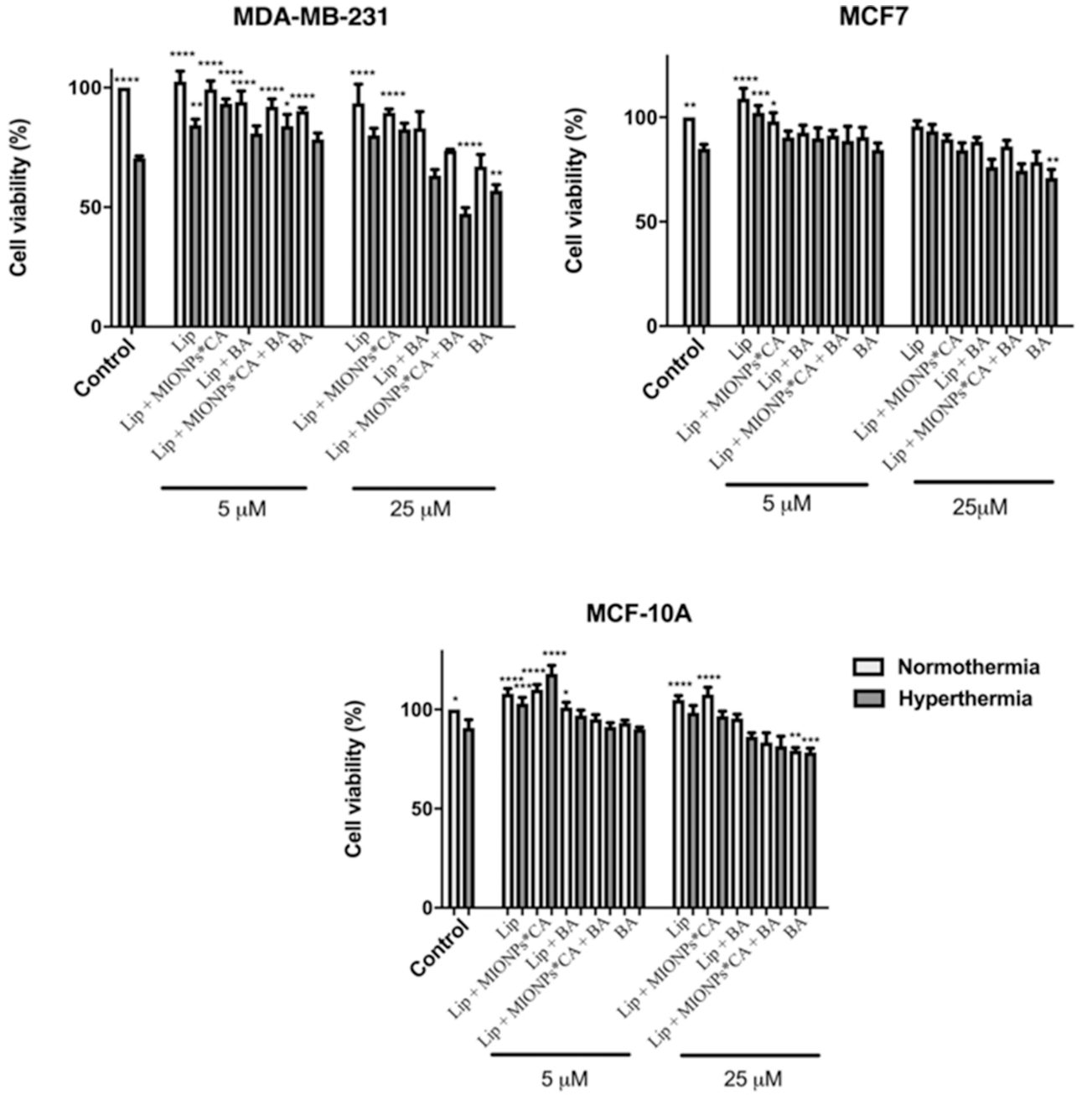

Figure 5 Viability percentages of breast adenocarcinoma (MDA-MB-231, MCF7) cells and breast epithelial (MCF 10A) cells after exposure to liposomal structures at concentrations of 5 and 25 μM. The MTT assessment was performed 24h post-stimulation, under normothermic (37 °C) and hyperthermic (43 °C) conditions. The cell viability percentage was normalized to control cells (no stimulation, under normothermic conditions). One-way ANOVA analysis was applied to determine the statistical differences followed by Tukey's multiple comparisons test vs hyperthermia control (*p < 0.05; **p < 0.01; ***p < 0.001, ****p < 0.0001). The data represent the mean values ± SD of three independent experiments (n=3).

control cells had normal, elongated shape and were adherent to the culture plate; BA-free nanoplatforms displayed no antiproliferative effect on the MDA-MB-231 cells migration rate under normothermic conditions, while Lip +MIONPs*CA+BA induced a slight inhibition. However, Lip+BA and Lip+MIONPs*CA+BA induced a decrease in confluency, which drastically suppressed the migratory potential of the invasive MDA-MB-231 cells, especially under hyperthermic conditions. MCF7 cell confluence decreased in the presence of liposomal structures containing BA (Lip+BA and Lip+MIONPs*CA+BA), under hyperthermic conditions. Comparing these results with the ones obtained for the MCF7 cells exposed to BA alone, it could be observed that Lip+BA and Lip

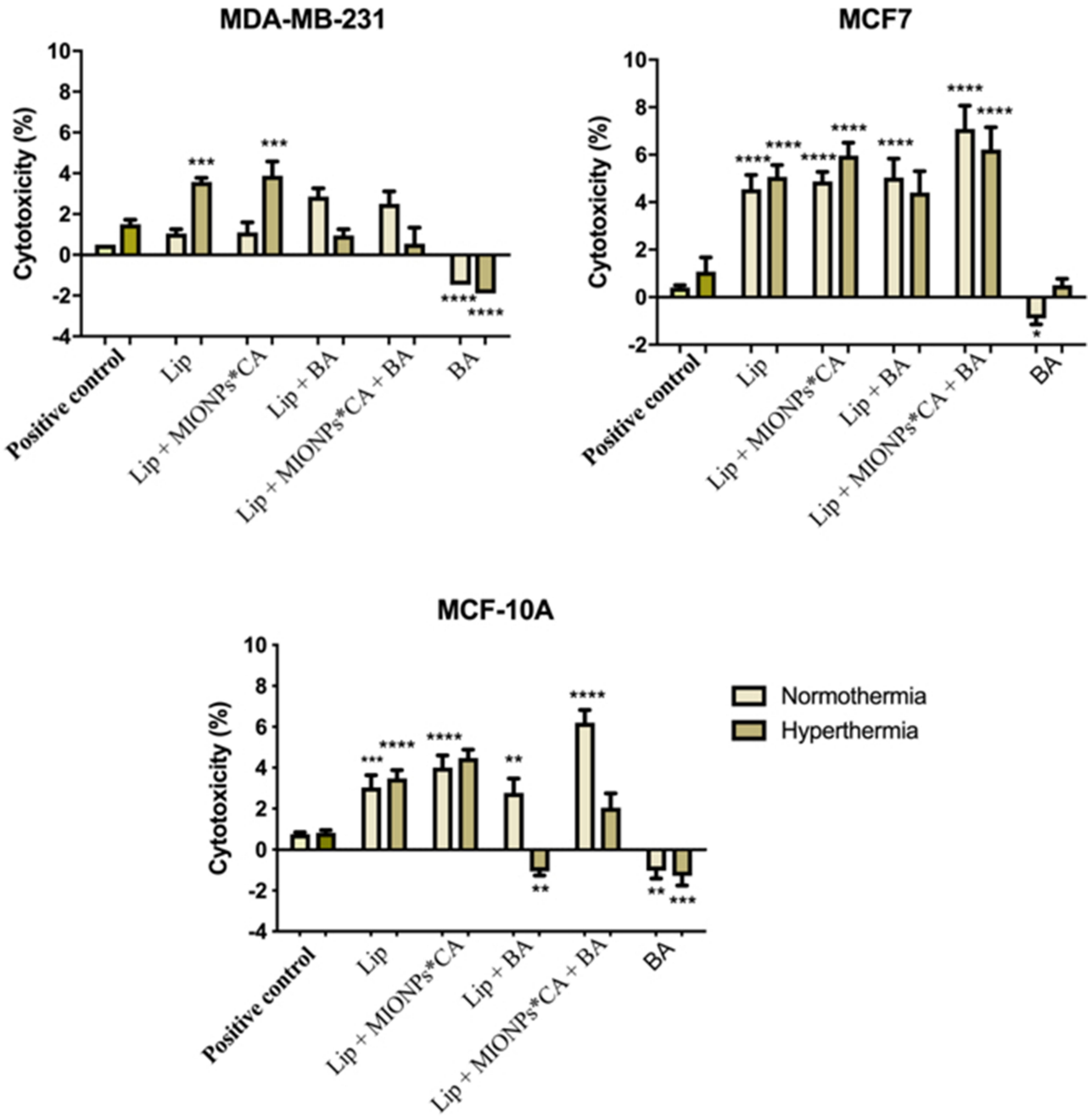

Figure 6 Cytotoxicity percentages of breast adenocarcinoma (MDA-MB-231, MCF7) cells and breast epithelial (MCF 10A) cells after exposure to liposomal structures at concentration of 25 μM. The LDH assessment was performed 24 h post-stimulation under normothermic (37 °C) and hyperthermic (43 °C) conditions. One-way ANOVA analysis was applied to determine the statistical differences followed by Tukey's multiple comparisons test vs hyperthermia control (*p < 0.05; **p < 0.01; ***p < 0.001, ****p < 0.0001). The data represent the mean values ± SD of three independent experiments (n=3).

+MIONPs*CA+BA induced a higher scratch closure percentage: 63.5% and 55.4%, respectively, versus 50.25% for BA alone, under hyperthermal treatment. The wound closure rate expressed by MCF 10A control cells (~40%) indicates that this cell line develops a lower migratory capacity, as compared to the adenocarcinoma cell lines (MDA-MB-231, MCF7), after 24 h. This may be explained by the low proliferative character of MCF 10A cells; thereby the effect may not be related to the test compounds treatment. However, all liposomal structures inhibited the migratory capacity of MCF-10A cells in a smaller proportion than the BA treatment; for BA-loaded magnetoliposomes (Lip+MIONPs*CA+BA) the wound closure rate was 49.59%, under normothermic

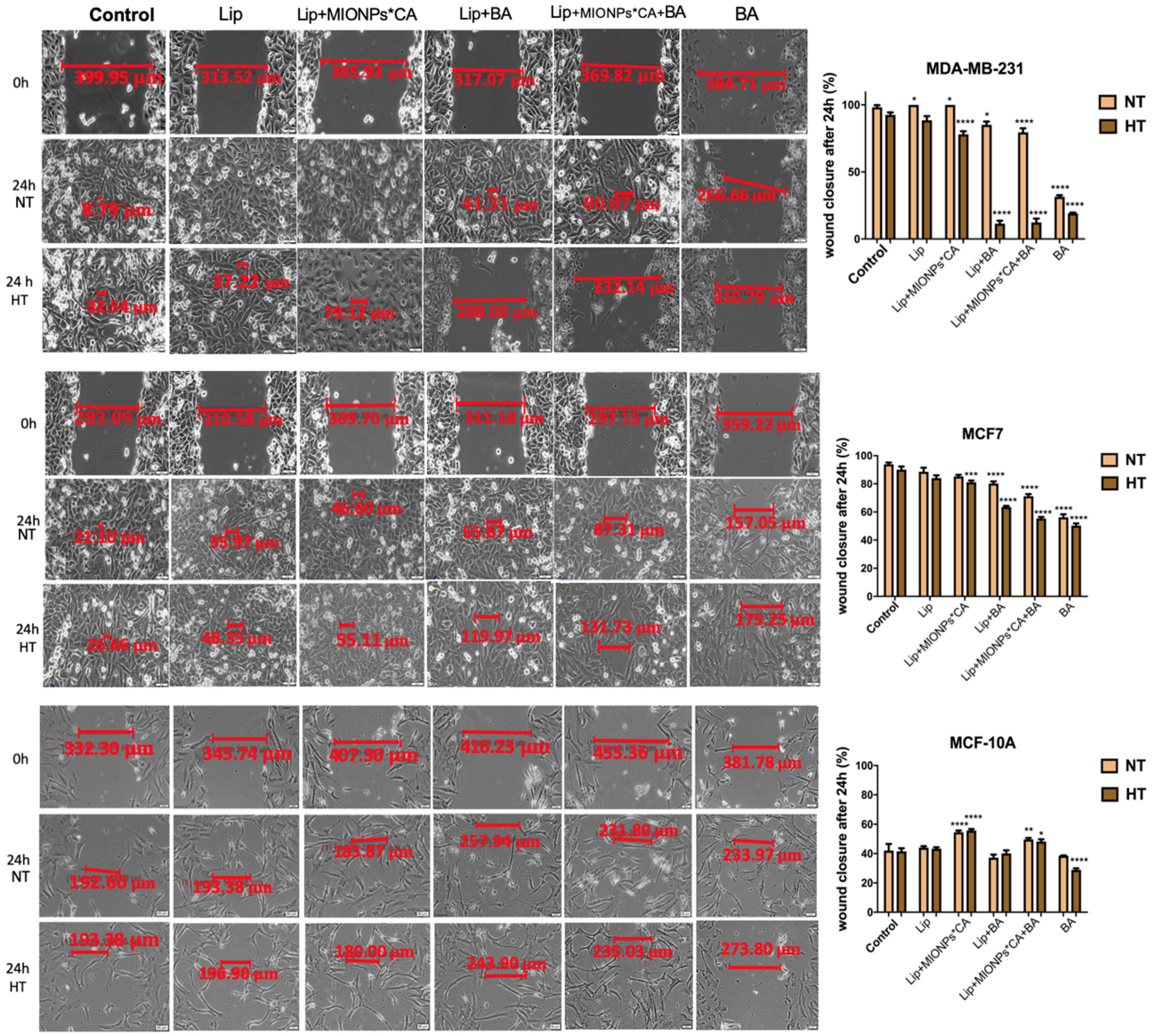

Figure 7 Representative images of the migratory capacity of the breast adenocarcinoma (MDA-MB-231, MCF7) cells and breast epithelial (MCF 10A) cells after treatment with test compounds at concentration of 25 μM. The results were expressed as percentage of wound closure after 24 h (normothermia/hyperthermia) compared to the initial surface; NT – normothermia (37 °C), HT – hyperthermia (43 °C). The cells were visualized by light microscopy, at magnification 20x. Scale bars represent 50 μm. One-way ANOVA analysis was applied to determine the statistical differences followed by Tukey's multiple comparisons test vs hyperthermia control (*$p < 0.05$; **$p < 0.01$; ***$p < 0.001$, ****$p < 0.0001$). The data represent the mean values ± SD of three independent experiments (n=3).

conditions and 48.9%, under hyperthermal treatment. Moreover, it could be observed that the hyperthermal treatment did not significantly affect the migratory capacity of MCF 10A cells when compared to control cells.

Nuclear and Microtubule Organization Determined by Immunofluorescence Assay

To obtain an insight into the mechanism of action exerted by BA-loaded magnetoliposomes (Lip+MIONPs*CA +BA) against breast adenocarcinoma (MDA-MB-231, MCF7) cells, under hyperthermic conditions, the cell morphology was further analyzed by immunofluorescence staining.

As presented in Figures 8 and 9, immunostaining of the cytoskeleton indicated that treatment with test compounds (25 μM) under hyperthermic conditions induced: i) chromatin condensation associated with nuclear disruption of MDA-MB-231 cells, massive nuclear growth of MCF7 cells after treatment with Lip+MIONPs*CA and also fragmentation of the centrosomes of both breast

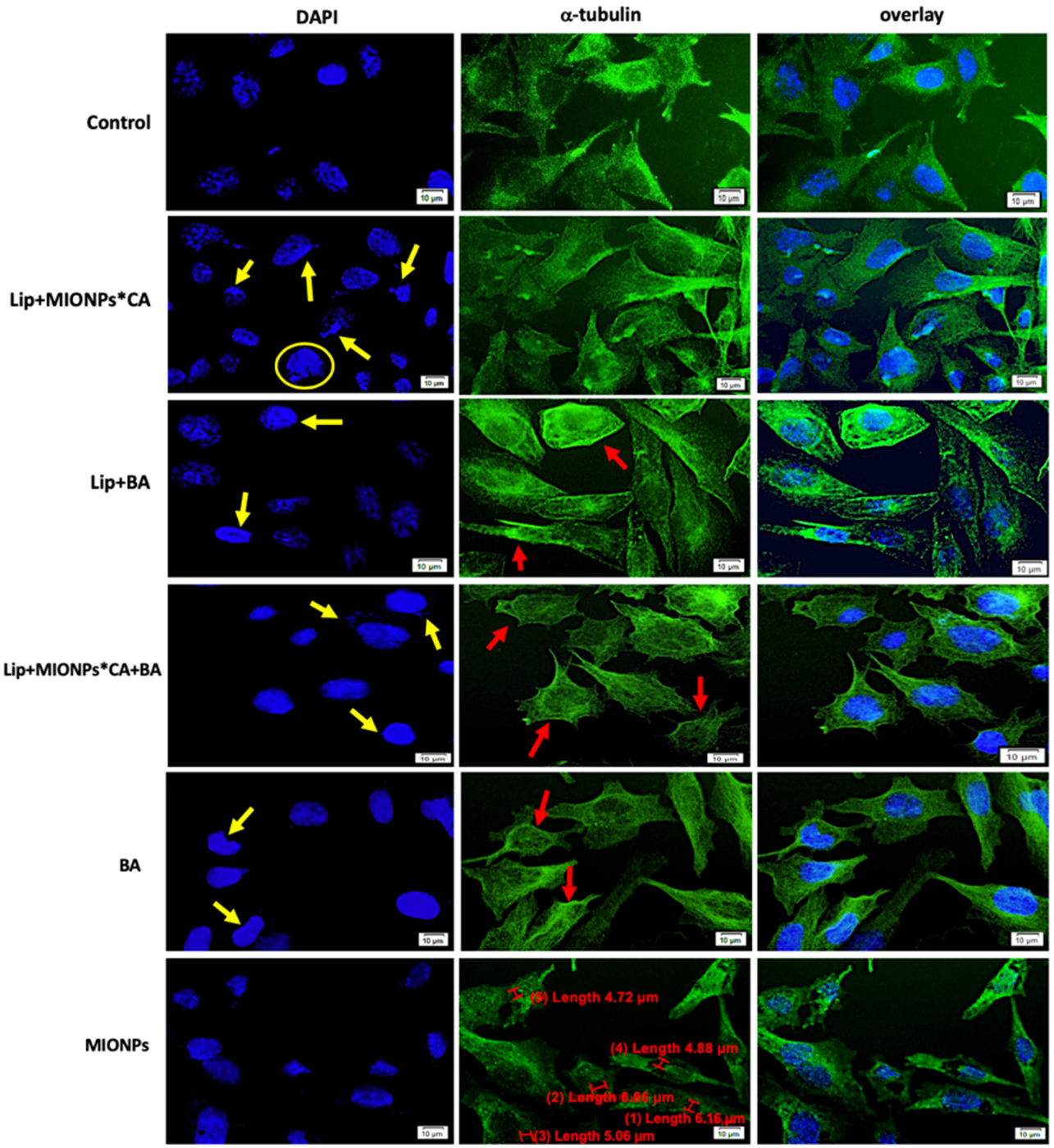

Figure 8 MDA-MB-231 cells visualized by fluorescence microscopy, after 24 h treatment with test compounds at concentration of 25 µM, under hyperthermal conditions. Nuclear and microtubules staining were expressed separately (DAPI and α-tubulin, respectively) and also combined (overlay). Yellow arrows marked the typical morphological changes for apoptosis induction: chromatin condensation, boundary alterations, and nuclear fragmentation, while enucleation process is highlighted by the yellow circle. The abnormal filamentous organization of microtubule (MT) network was indicated by the red arrows. Three independent experiments were performed for each sample (n=3).

adenocarcinoma cell lines; ii) chromatin condensation in both cell lines, along with disruption of the MT assembly in MDA-MB-231 cells and extensive depolymerization in MCF7 cells after exposure to Lip+BA; iii) chromatin condensation in both cell lines, associated with nuclear membrane blebbing of MDA-MB-231 cells after treatment with Lip+MIONPs*CA+BA and in the case of MCF7 cells, microtubule bundles were

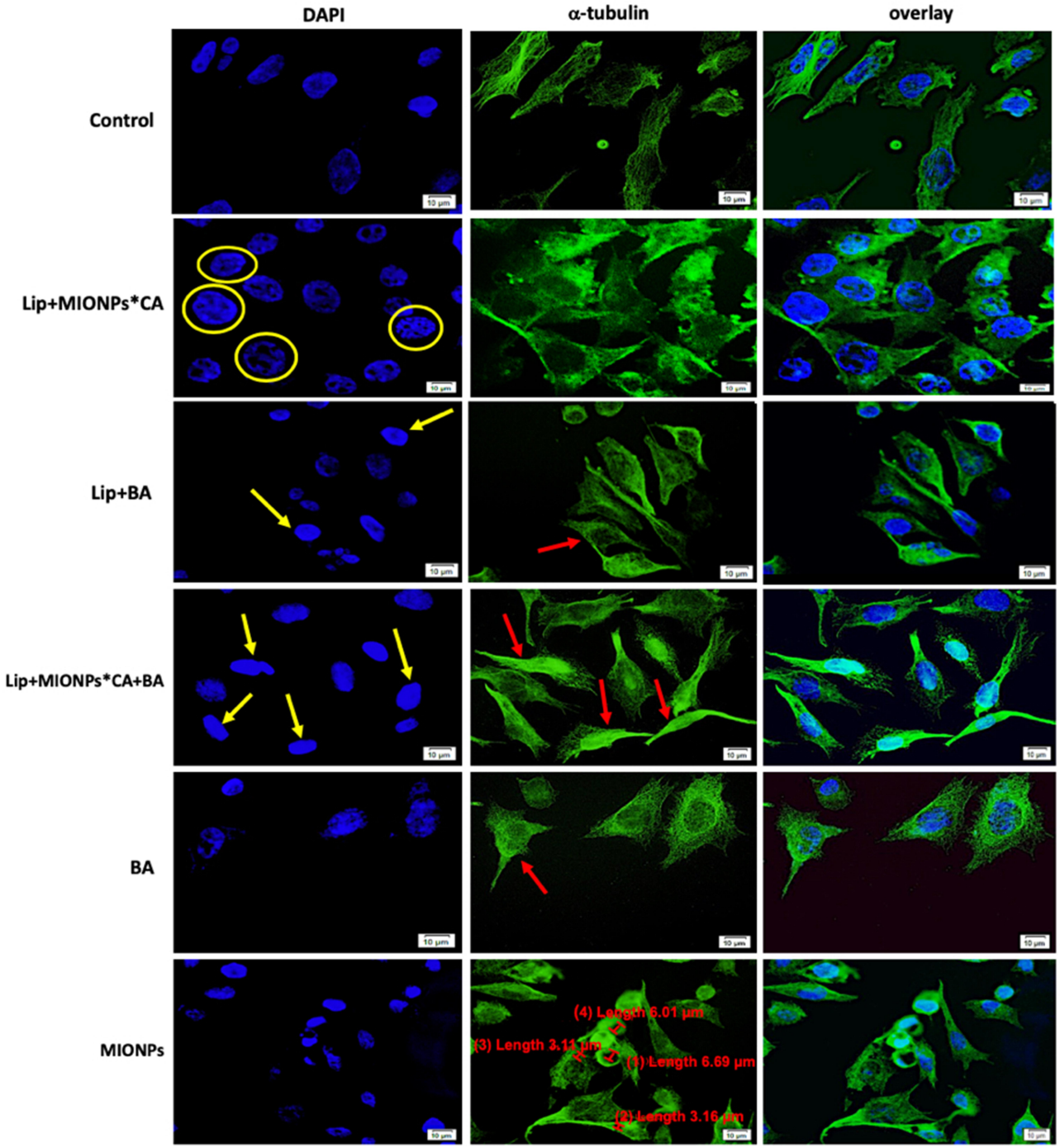

Figure 9 MCF7 cells visualized by fluorescence microscopy, after 24 h treatment with test compounds at concentration of 25 μM under hyperthermal conditions. Nuclear and microtubules staining were expressed separately (DAPI and α-tubulin, respectively) and also combined (overlay). Yellow arrows marked the typical morphological changes for apoptosis induction: chromatin condensation, boundary alterations, and nuclear fragmentation, while enucleation process is highlighted by the yellow circle. The abnormal filamentous organization of microtubule (MT) network was indicated by the red arrows. Three independent experiments were performed for each sample (n=3).

noticed; iv) chromatin condensation and alterations of MDA-MB-231 cell nuclei morphology after stimulation with BA; v) MIONPs accumulation within the cells with alterations of the cytoskeleton only when high MIONPs uptake occurred. Depending on the type of the tumor cell line, MIONPs was accumulated in different concentrations (Figures 8 and 9).

Some changes are also observed in the hyperthermia control cells, which are most likely induced by the hyperthermic treatment applied. The quantification of

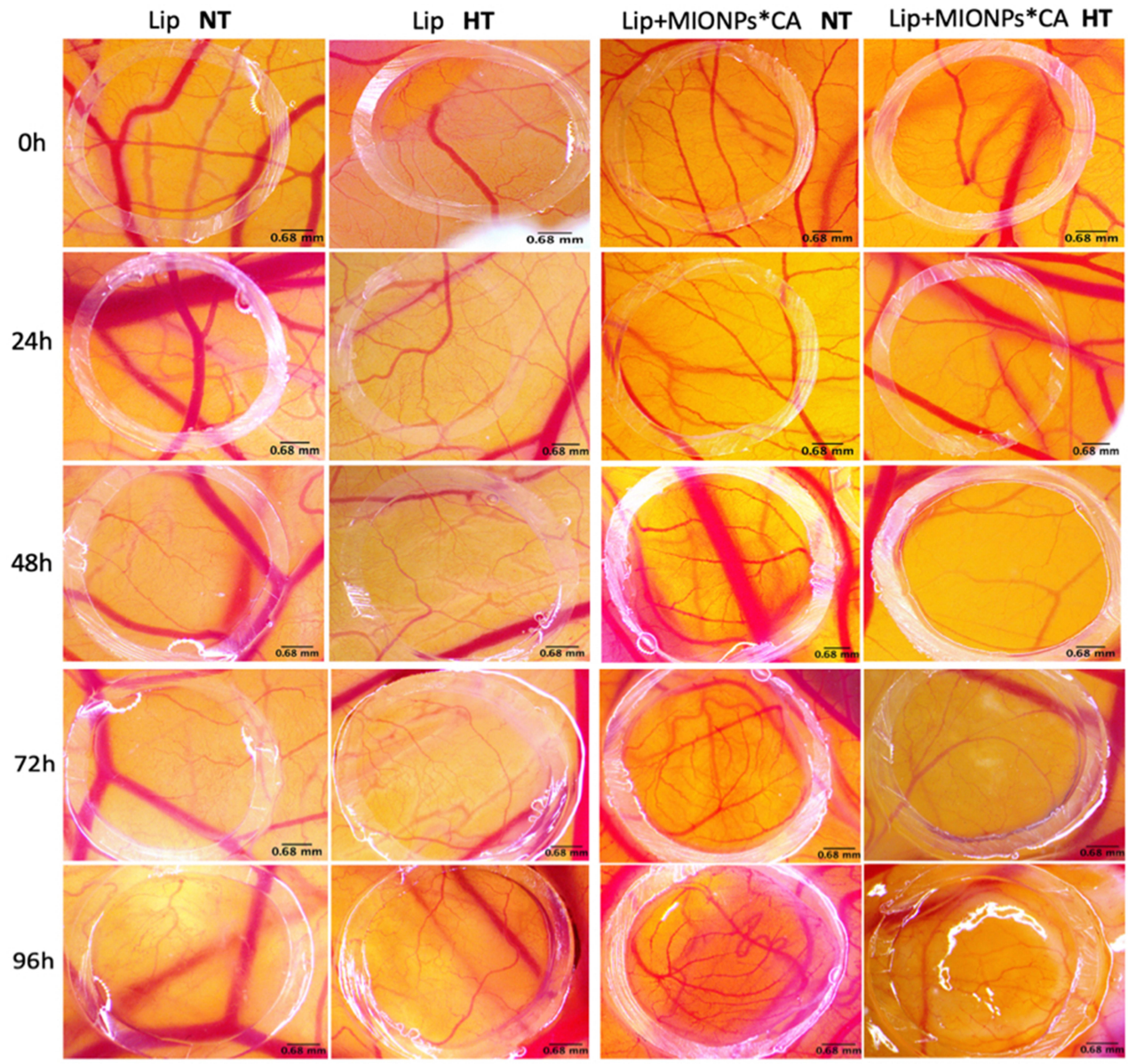

Figure 10 Stereomicroscopic in ovo images of the vascularized areas treated with blank liposomal samples (Lip and Lip+MIONPs*CA) at concentration of 25 μM, under normothermic – NT (37 °C) and hyperthermic pre-treatment – HT (46 °C). Three independent experiments were performed for each sample (n=3).

abnormal changes index of each sample compared to control hyperthermia can be consulted in Figure S2.

In ovo Angiogenesis Assessment

In the present study, the CAM assay was performed in order to evaluate the potential anti-angiogenic effect of the liposomal samples under normothermic and hyperthermic conditions. The results obtained for liposomal samples without BA (Lip, Lip+MIONPs*CA) are presented in Figure 10, whereas the activity expressed by liposomal samples containing BA (Lip+BA and Lip+MIONPs*CA +BA) is depicted in Figure 11.

BA-free liposomal samples (Lip, Lip+MIONPs*CA) both under normothermic and hyperthermic conditions were well tolerated, and the treated specimens registered good viability. When analyzing the modification induced 48 h, 72 h and 96 h after the inoculation of the samples, some differences were noted concerning both the BA-free liposomal samples and the conditions that preceded the application. Liposomes alone did not induce major changes in the aspect of the vascular developing plexus, as fine vessels with moderate branching patterns were observed especially for the hyperthermia exposed sample. The other blank liposomal sample, containing Lip

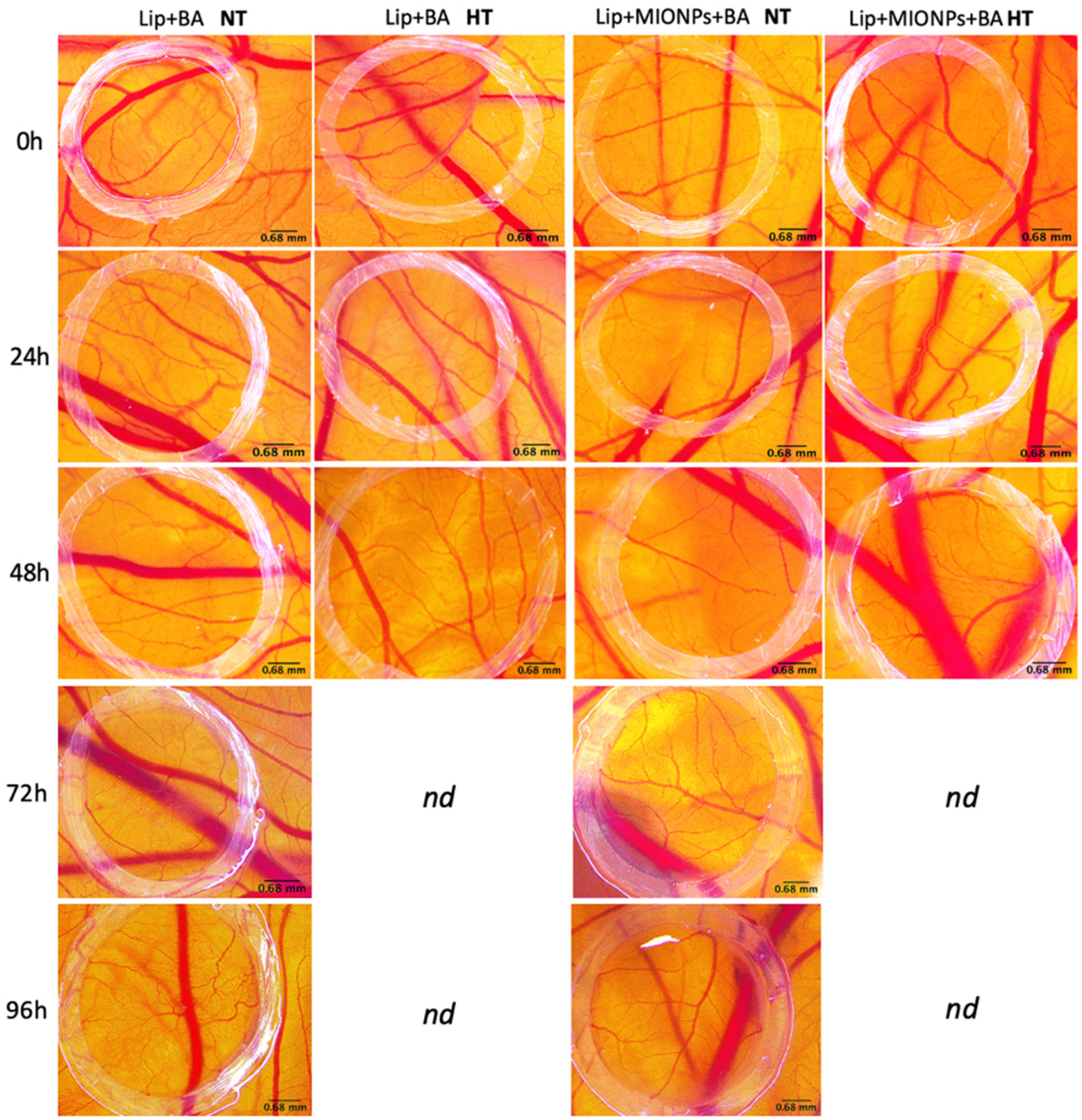

Figure 11 Stereomicroscopic in vivo images of the vascularized areas treated with liposomal samples containing BA (Lip+BA and Lip+MIONPs*CA+BA) at concentration of 25 μM, under normothermic - NT (37 °C) and hyperthermic pre-treatment - HT (46 °C). The specimens with hyperthermic pre-treatment died after 48h, so they were not determined (nd) further. Three independent experiments were performed for each sample (n=3).

+MIONPs*CA, did not affect the angiogenic process under normal conditions, while under hyperthermia pre-treatment, the vessel architecture seemed slightly affected, showing a lower number of small interconnected capillaries.

While analyzing the effects induced on the CAM angiogenesis by BA-loaded liposomes, Lip+BA and Lip +MIONPs*CA+BA, we noted that under normothermic conditions, the viability was comparable to the blank specimens and no important inhibitory effects upon the angiogenesis process were registered 48 h after inoculation (Figure 11). Still, the density of new forming capillaries was slightly lower for the Lip+BA treated specimens, compared to Lip+MIONPs*CA+BA. Regarding the hyperthermia pretreated samples containing BA, we noted a lower viability of the specimens, up to 48 h,

suggesting that higher incubation periods (72 h and 96 h) may lead to angiogenesis impairment and consequently to the death of the specimens.

The most representative results in terms of angiogenesis inhibition were quantified and are presented in Figure S3.

Discussion

The present study describes the development of a multifunctional vesicular nano-system, using BA and magnetic iron oxide nanoparticles (MIONPs) as therapeutic agents. A liposomal nanoplatform was selected as the most adequate carrier for both BA and MNPs due to its more difficult identification by macrophages compared to stiff particles.[60] The cytotoxic effect induced by BA on the tumor microenvironment was investigated under hyperthermic conditions, considering previous reports of Wachsberger et al[61] who concluded that hyperthermia facilitated an augmented therapeutic effect. MIONPs*CA colloidal suspension has already been tested and manifested promising results under hyperthermic conditions against the highly aggressive breast cancer MDA-MB -231 cells.[62]

Synthesis of liposomal structures was accomplished by the thin film hydration method, which is considered to be the most effective method for entrapping hydrophobic compounds.[30] Sonication and extrusion through membranes with a certain porosity size are some of the well-established methods to obtain nanosized liposomes with a uniform size distribution.[63] Accordingly, following membrane extrusion, unilamellar vesicles with a uniform distribution size range (<200 nm) were obtained, which were subsequently confirmed by DLS analysis (Table 1).

Nevertheless, several aspects have been considered to achieve stable thermosensitive liposomes. Firstly, selecting the optimal HSPC:Chol ratio has played a major role; literature shows that soybean phosphatidylcholine provides a good entrapment rate of the chemotherapeutic agent and may even influence the membrane of certain tumor cells.[64,65] Moreover, the licensing of Lipoplatin™, phosphatidylcholine:cholesterol-based formulation[64] and the successful development of two BA-loaded liposomal platforms using the same lipid combination (phosphatidylcholine:cholesterol)[37,66] have strongly supported the lipid structure selection for this study. The addition of cholesterol to the phospholipid bilayer grants the liposomal structure the optimal stiffness to avoid the drain of hydrophilic molecules.[30,67] However, the ratio must be carefully selected based on the fact that any excess could lead to a competition with the lipophilic drug, BA in our case, for the free encapsulation space within the phospholipid bilayer.[65] Secondly, entrapping a stable MIONPs colloidal suspension within the inner aqueous core of the liposomes was mandatory in order to avoid interactions with the phospholipid bilayer.[28] Thirdly, the functionalization of the liposome surface with PEG-2000 led to the so-called "stealth liposomes", which are known to reduce the clearance rate and to improve liposomal steric stability.[67,68] The addition of PEG-2000 on liposomes surfaces may increase their encapsulation efficiency rate and delay the oxidation process, which in turn enhances their physical stability and avoids drug leakage during long time storage.

The stability of nano-formulations for use in the biomedical field is one of the most significant parameters, in particular for liposomes; extremely negative or positive values of zeta potential are associated with a strong repulsion between particles thereby avoiding agglomeration and increase of nanoparticle diameter. In general, particles with a zeta potential more positive or more negative than 20 mV are considered to be stable.[51] The ζ-potential of all liposomal structures (Lip, Lip+MIONPs*CA, Lip+BA, Lip+MIONPs*CA+BA) indicated appropriate stability; in addition, all liposomal samples displayed a mean diameter below 200 nm (Table 1), enabling their tumor accumulation through the EPR effect.[66]

Another important parameter for biomedical applications is the superparamagnetic behavior of MNPs which enables their magnetization depending on the presence of an external magnetic field.[10,16] In this regard, the saturation magnetization of both types of magnetoliposomes (Lip+MIONPs*CA, Lip+MIONPs*CA+BA) was evaluated. However, a decrease of the magnetization potential was observed in the case of magnetoliposomes if compared to the MIONPs. This fact can be correlated to the lack of magnetic properties exhibited by the CA and the double phospholipid layers that cover the iron oxide core.[26] Besides the superparamagnetic feature, the heat transfer described by the ILP analysis of MIONPs indicates the possibility of their use in magnetic heat generation. Nevertheless, to exhibit a cytotoxic effect, MNPs must be embedded by the tumor cells and in the presence of an AMF, hyperthermal conditions could be achieved due to Néel or/and Brownian relaxation.[69,70]

Regarding the hyperthermic treatment (43 °C) used for the in vitro experiments, a difference of 3 °C can be

noticed between the thermal set-up employed for in vitro experiments and the phase transition of BA-loaded magnetoliposomes. The temperature selection was based on previous literature reports on the strong correlation between the heating efficacy of tumors through magnetic hyperthermia and the distribution of the magnetic material within the tumor;[71] thus, even if at the injection site the temperature of the tumor would reach 46 °C and could, in our case, ensure the transition temperature of the liposomes, the average temperature of the tumor cells will be several degrees below, considered in the present study to be around 43 °C. Therefore, the current in vitro experiments simulates the corresponding conditions that could occur in vivo. Still, in order to obtain the mandatory thermal parameters, the 43 °C cumulative equivalents minutes (CEM43) protocol was employed,[41] by maintaining the cells for 90 min at 43 °C, a temperature treatment that corresponds to 30 min at 46 °C.[9]

However, for the in ovo assessments all liposomal samples were previously maintained at 46 °C, to ensure the liposomal membrane destruction and the release of BA, because in ovo specimens cannot be subjected to hyperthermia due to embryos death.

The clinical application of magnetically induced hyperthermia is considered to be achieved by intratumoral injection of magnetic nanoparticles able to induce heat when an external magnetic field is applied. To induce the appropriate cytotoxic thermal conditions, the concentration of magnetic material administrated at the tumor site depends on the size of the targeted carcinoma.[17]

Regarding the cytotoxicity of the magnetoliposomes and controls, different responses of the MDA-MB-231 and MCF7 cell lines were recorded, depending on the thermal parameters employed (normothermia vs hyperthermia).

These different responses may be correlated with two aspects: i) the distinctive morphological phenotype of the two breast adenocarcinoma cell lines which respond differently to the same treatment, and ii) the distinct iron accumulation ability expressed by the selected cell lines. Our group already reported that MIONPs are cytotoxic against tumor melanoma cells, generating different responses depending on the cell origin, phenotype and metastatic potential.[72–74] The stronger BA cytotoxic effect on MDA-MB-231 cells versus MCF7 cells could explain the difference in cell viability percentages induced by the BA-loaded nanoplatforms when applied on the two breast adenocarcinoma cell lines. In terms of hyperthermia effects, it could be noticed a decrease in the MDA-MB -231 cell population when treated with BA-loaded nanoformulations, compared to the same treatment groups under normothermic conditions. This result may be explained by the thermosensitive feature of liposomes, which release BA only after reaching the transition temperature of the phospholipid bilayer, whereas under normothermic conditions BA is still entrapped within the liposomes and cannot exert its anti-tumor effect. Thus, the stronger cytotoxic effect induced by the BA-loaded magnetoliposomes under hyperthermic conditions, compared with the effect induced by BA-free liposomes under the same thermal conditions can be attributed to the BA content; however, a limited release of BA from liposomes may occur due to the extremely hydrophobic nature of BA, which exhibits a much higher affinity for the lipophilic part of the liposomes than for the hydrophilic biological environment. This drawback should be overcome by the in vivo administration of the nano-platforms that, once subjected to enzymatic metabolism, will presumably lead to an enhanced BA release. A similar phenomenon was previously reported by our group when BA and its analog – betulin – were incorporated within gamma-cyclodextrin derivatives decorated with long hydrophobic chains which provided excellent encapsulation efficacy.[75,76] While the in vitro experiments displayed poor cytotoxic effects due to the high stability of the cyclodextrin-drug complex and its inability to release the active drug, the in vivo testing on animal models revealed a strong antitumor activity.

Nevertheless, the viability rates of MDA-MB-231 cells exposed to BA-loaded liposomal nano-platforms, under hyperthermic conditions, were reduced when compared to hyperthermia control cells. This supports the conclusion that hyperthermia treatment alone was not the only factor responsible for the cytotoxic effect, but instead, there is a combined, enhanced cytotoxic effect induced by hyperthermia and BA together. However, for MCF7 cells, hyperthermia did not play an important role in decreasing cell viability, and moreover, BA itself manifested a less intense cytotoxic activity compared to the effect exerted on MDA-MB-231 cells.

When comparing our results with Doxorubicin (Dox), a broad-spectrum anti-tumor agent that is generally considered the most effective single compound for the treatment of breast cancer,[7] it was noticed that the concentration of Dox required to induce significant cell death of breast adenocarcinoma cells is lower than the

concentration of our newly developed nanoplatforms. According to Pilco-Ferreto et al,[77] the concentration of 8 μM Dox induced a 50% reduction of MDA-MB-231 cell viability after 24-h post-exposure. However, the viability of non-tumorigenic immortalized breast epithelial MCF 10F cells decreased by 30% after treatment with a concentration of 2 μM Dox, revealing high cytotoxicity on normal cells, thus highlighting the side effects. Therefore, even if in the case of our newly developed formulation a higher molecular concentration of the active substance (25 μM - BA) is needed to induce a similar anti-tumor effect, this concentration affects a much smaller proportion of healthy cells, being one of the main advantages of these nanoformulations.

As previously reported, the mechanism of action for BA consists of affecting the cell mitochondrial activity,[23] which is an intracellular process that cannot be well quantified through the LDH method.[59] Moreover, Zheng et al showed in a recent study that BA acts as an inhibitor on aerobic glycolysis, especially on highly aggressive breast cancer cells, and correlated this result to a low lactate production.[78] This report may explain the absence of LDH release and the negative cytotoxic effect noticed for BA-treated cells (Figure 6); also, it may justify the different results obtained through MTT vs LDH assays, for BA-loaded platforms.

As the migratory potential of tumor cell lines is known to play a key role in tumor proliferation, the evaluation of BA-loaded magnetoliposomes and controls as anti-migratory agents was employed in this study, by applying a wound healing technique. The results obtained through this assessment corroborated the MTT data, revealing that BA-loaded nano-platforms applied under normothermic conditions did not induce a significant inhibitory activity on the migratory potential of the MDA-MB-231 and MCF7 cells; whereas, under hyperthermic conditions, the proliferative activity of the breast adenocarcinoma cell lines was strongly inhibited, especially for the highly invasive MDA-MB-231 cells. The non-tumorigenic breast epithelial MCF 10A cells exposed to BA-loaded platforms and control samples presented almost the same migratory and proliferative activity as the control cells; however, a slight inhibitory effect was induced by BA alone under hyperthermic treatment.

Another factor that influenced the cytotoxic activity of the magnetoliposomes was the accumulation rate of MIONPs; MCF7 cells expressed a lower uptake rate, compared to MDA-MB-231 cells. In the present study, MIONPs accumulation within both breast adenocarcinoma cell lines was emphasized by immunofluorescence, followed by measurements of iron agglomerates within the cells (Figures 8 and 9). Results revealed that the iron bundles were much higher (6.88 μm in diameter) within MDA-MB-231 viable cells, whereas iron clusters detected within MCF7 viable cells displayed a diameter of only 3.16 μm (when iron assembled in groups with a diameter around 6 μm, MCF7 cells shrink and become round, showing specific signs of apoptosis). Based on these results, it could be concluded that the iron accumulation rate is reduced to half in MCF7 cells, compared to MDA-MB-231 cells. Our results are in agreement with other recent studies.[39,79] The difference in iron accumulation rate between the two breast adenocarcinoma cell lines could be explained by a more intensive metabolic activity of MDA-MB-231 cells, compared to MCF7 cells, which may have stimulated the membrane receptors expression, leading to a higher iron internalization.[79] Besides the cell phenotype and the modification of the expression of cell membrane receptors under Fe treatment, the endocytosis pathway may also be influenced by the physico-chemical properties (size, shape, surface charge) of internalized Fe NPs.[39,79,80] In order to obtain more information about the mechanism of action of magnetoliposomes and controls, the cytoskeleton changes of both breast adenocarcinoma lines (MDA-MB-231 and MCF7) were ascertained, under hyperthermal conditions.

The microtubule (MT) assembly plays a key role in cytoskeleton dynamics, orchestrating important cellular processes such as organization and distribution of mitotic spindle and organelles (Golgi complex, endoplasmic reticulum), cell shape maintenance and intracellular transportation via MT-motor proteins (kinesins), proteins which also regulate the MT dynamics.[81–83] Modifications of the MTs network may alter cell division by inducing cell cycle arrest and causing cell death, which promotes MTs as an effective target in cancer chemotherapy. Tubulin assembly modulator compounds are divided into two major groups: i) MT-stabilizing agents (ie, Paclitaxel), which stimulate tubulin polymerization and block MT dynamics, leading to MT bundles in interphase cells and increased MTs density; and ii) MT-destabilizing agents (ie, colchicine and vinca alkaloids), which strongly inhibit MTs assembly and induce cell cycle arrest in mitosis phase by triggering tubulin depolymerization.[82,84–86] The present results indicate that adenocarcinoma cell lines (MDA-MB-231, MCF7) stimulated with the magnetoliposamal samples

and controls experienced nuclear and MT network alterations, under hyperthermic conditions. Both cell lines treated with Lip+MIONPs*CA presented extensive cell nuclear enlargement, a specific sign of enucleation. The enucleation process occurs when cellular nuclei increase their size until the nuclear extrusion process emerged[87] and the cytoplasmic compartment became more compact.[88] This phenomenon was previously identified on SK-BR-3 and MCF7 cells by Paunescu et al[89] following stimulation with MIONPs obtained by the combustion method.

Lip+BA caused disruption of the MT assembly in MDA-MB-231 cells and depolymerization in MCF7 cells by acting like an MT-destabilizing compound on MCF7 cells, whereas Lip+MIONPs*CA+BA produced blebbing and shape alterations of MDA-MB-231 cell nuclei membrane, along with tubulin polymerization of MCF7 cells, thereby creating MT bundles, which hampered MT dynamics.

Regarding the angiogenesis process, the hyperthermia pretreated samples containing BA induced lower viability of the specimens (48 h) compared to BA-loaded nanoplatform under normothermic conditions (more than 96 h). Higher incubation periods (72 h and 96 h) with hyperthermia pretreated BA-loaded samples could be correlated with angiogenesis impairment causing embryos death (Figure 11). Our previously reported effects of BA alone or contained in nano-emulsions indicated an indirect mechanism of action, altering the maturation period of the newly forming vessels.[90] The impact upon vessel development during a peak in the angiogenic process at this stage of incubation[91] might be stronger, with higher inhibitory effects, due to enhanced bioavailability of BA, and possibly in conjunction with the entire liposomal formulation, based on the so-called EPR effect.[92] An important inverse correlation between angiogenesis and survival rate in the case of invasive breast cancer describes the disease as an angiogenesis-dependent malignancy.[93] Thus, angiogenesis inhibitors with an optimal bioavailability and safety profile are highly needed. Bioactive natural compounds such as BA represent a valuable path of investigation for advances in the control of metastatic breast cancer.

One of the most important features of any anti-cancer agent is represented by its high selective toxicological profile, manifesting high toxicity on tumor cells and low toxicity on healthy cells. In this regard, the selective cytotoxic effect expressed by BA-loaded magnetoliposomes on human breast cell lines must be pointed out for the perspective of their development as tools in a novel therapeutic approach to invasive breast cancer.

Liu et al developed two types of liposomes containing BA: PEGylated BA liposomes, which improved BA bioavailability,[66] and gold nano-shell-based betulinic acid liposomes, considered suitable structures for both chemo and photothermal therapy.[37] Nevertheless, BA-loaded magnetoliposomes were developed and reported for the first time by our group.[94,95]

The present study provides preliminary data on MIONPs' behavior, under hyperthermic conditions. However, improving superparamagnetic characteristics and heat dissipation capacity of magnetoliposomes are some of the challenges raised by this study, to which our group will address in the upcoming studies, together with an advanced biological screening using three-dimensional (3D) human breast carcinoma spheroids under hyperthermic conditions, which will grant us the opportunity to generate a heat map of the 3D spheroids, that could be further used as preliminary data for in vivo experiments performed under magnetically induced hyperthermia.

Conclusion

The present study reported the synthesis process and physico-chemical characterization of the multifunctional BA-loaded magnetoliposomes, along with a complex in vitro and in ovo biological profile. The synthesized BA-loaded magnetoliposomes present a diameter suitable for biological purposes of around 198 nm, superparamagnetic behaviour, magnetically induced heat capacity and biocompatible phase transition temperature of the lipid bilayer; thus, all the mandatory features that make these structures ideal candidates for both hyperthermia-inducing and remote control drug release are met. Under hyperthermal treatment, BA-loaded magnetoliposomes manifested enhanced anti-tumor activity compared to BA and BA-loaded liposomes under normothermic or hyperthermic conditions and MIONPs-loaded liposomes at a concentration of 25 μM induced impairment of human breast adenocarcinoma cells, correlated to the enucleation process in MCF7 cells and DNA fragmentation in MDA-MB-231 cells. Moreover, the entrapped-MIONPs played an essential role in the anti-cancer activity of the BA-loaded magnetoliposomes, leading to an enhanced cytotoxic effect, compared to MIONPs-free liposomes containing BA. Collectively, these findings could be important features for the development of a new and

innovative breast cancer therapeutic approach, by merging the anti-tumor activity of BA with hyperthermal treatment. Therefore, future directions regarding advanced screening of the multifunctional nanoplatforms are considered.

Acknowledgments

This paper was published under the frame of European Social Found, Human Capital Operational Programme 2014–2020, project no. POCU/380/6/13/125171. Claudia G. Farcas (Watz) acknowledges also the financial support from the doctoral research project; contract no 1531/2/18.01.2019, 2464/1/17.01.2020. V. Socoliuc acknowledges the financial support from Romanian Academy – Timisoara Branch 2016–2020 research programme.

The authors are grateful to "George Emil Palade" Electron Microscopy Center, Institute of Life Sciences, "Vasile Goldis", Western University of Arad, particularly to PhD Ciprian-Valentin Mihali for performing the SEM-EDAX analysis. All in vitro experiments were conducted within the Center of Pharmaco-toxicological evaluations from the Faculty of Pharmacy, "Victor Babes" University of Medicine and Pharmacy, Timisoara.

Author Contributions

All authors contributed significantly to the present study, whether that is in the conceptualization, study design, investigation, acquisition of data, analysis and interpretation, or took part in drafting, revising or critically reviewing the article. All authors gave final approval of the current version to be published, all authors agreed on the journal to which the article has been submitted and all authors also agree to be accountable for all aspects of the work.

Disclosure

The authors report no conflicts of interest in this work.

References

1. Temian DC, Pop LA, Irimie AI, Berindan-Neagoe I. The epigenetics of triple-negative and basal-like breast cancer: current knowledge. *J Breast Cancer*. 2018;21(3):233–243. doi:10.4048/jbc.2018.21.e41
2. Braicu C, Chiorean R, Irimie A, et al. Novel insight into triple-negative breast cancers, the emerging role of angiogenesis, and antiangiogenic therapy. *Expert Rev Mol Med*. 2016;18:e18. doi:10.1017/erm.2016.17
3. WHO. Breast cancer: prevention and control; 2020. Available from: https://www.who.int/cancer/detection/breastcancer/en/. Accessed October 8, 2020.
4. Bandyopadhyay S, Bluth MH, Ali-Fehmi R. Breast carcinoma: updates in molecular profiling 2018. *Clin Lab Med*. 2018;38(2):401–420. doi:10.1016/j.cll.2018.02.006
5. Hurvitz S, Mead M. Triple-negative breast cancer: advancements in characterization and treatment approach. *Curr Opin Obstet Gynecol*. 2016;28(1):59–69. doi:10.1097/GCO.0000000000000239
6. Lovitt CJ, Shelper TB, Avery VM. Doxorubicin resistance in breast cancer cells is mediated by extracellular matrix proteins. *BMC Cancer*. 2018;18(1):41. doi:10.1186/s12885-017-3953-6
7. AbuHammad S, Zihlif M. Gene expression alterations in doxorubicin resistant MCF7 breast cancer cell line. *Genomics*. 2013;101(4):213–220. doi:10.1016/j.ygeno.2012.11.009
8. Kobayashi T. Cancer hyperthermia using magnetic nanoparticles. *Biotechnol J*. 2011;6(11):1342–1347. doi:10.1002/biot.201100045
9. Kossatz S, Grandke J, Couleaud P, et al. Efficient treatment of breast cancer xenografts with multifunctionalized iron oxide nanoparticles combining magnetic hyperthermia and anti-cancer drug delivery. *Breast Cancer Res*. 2015;17:66. doi:10.1186/s13058-015-0576-1
10. Gupta AK, Gupta M. Synthesis and surface engineering of iron oxide nanoparticles for biomedical applications. *Biomaterials*. 2005;26(18):3995–4021. doi:10.1016/j.biomaterials.2004.10.012
11. Nguyen VTA, De Pauw-gillet M-C, Gauthier M, Sandre O. Magnetic polyion complex micelles for cell toxicity induced by radiofrequency magnetic field hyperthermia. *Nanomater (Basel, Switzerland)*. 2018;8(12). doi:10.3390/nano8121014
12. Kulshrestha P, Gogoi M, Bahadur D, Banerjee R. In vitro application of paclitaxel loaded magnetoliposomes for combined chemotherapy and hyperthermia. *Colloids Surf B Biointerfaces*. 2012;96:1–7. doi:10.1016/j.colsurfb.2012.02.029
13. Deatsch A, Evans B. Heating efficiency in magnetic nanoparticle hyperthermia. *J Magn Magn Mater*. 2014;354:163–172. doi:10.1016/j.jmmm.2013.11.006
14. Tombacz E, Turcu R, Socoliuc V, Vekas L. Magnetic iron oxide nanoparticles: recent trends in design and synthesis of magnetoresponsive nanosystems. *Biochem Biophys Res Commun*. 2015;468(3):442–453. doi:10.1016/j.bbrc.2015.08.030
15. Nguyen D, Kim K. Controlled synthesis of monodisperse magnetite nanoparticles for hyperthermia-based treatments. *Powder Technol*. 2016;301:1112–1118. doi:10.1016/j.powtec.2016.07.052
16. Bakhtiary Z, Saei AA, Hajipour MJ, Raoufi M, Vermesh O, Mahmoudi M. Targeted superparamagnetic iron oxide nanoparticles for early detection of cancer: possibilities and challenges. *Nanomedicine*. 2016;12(2):287–307. doi:10.1016/j.nano.2015.10.019
17. Fortes Brollo ME, Dominguez-Bajo A, Tabero A, et al. Combined magnetoliposome formation and drug loading in one step for efficient alternating current-magnetic field remote-controlled drug release. *ACS Appl Mater Interfaces*. 2020;12(4):4295–4307. doi:10.1021/acsami.9b20603
18. Linh PH, Phuc NX, Hong LV, et al. Dextran coated magnetite high susceptibility nanoparticles for hyperthermia applications. *J Magn Magn Mater*. 2018;460:128–136. doi:10.1016/j.jmmm.2018.03.065
19. Jadhav NV, Prasad AI, Kumar A, et al. Synthesis of oleic acid functionalized Fe3O4 magnetic nanoparticles and studying their interaction with tumor cells for potential hyperthermia applications. *Colloids Surf B Biointerfaces*. 2013;108:158–168. doi:10.1016/j.colsurfb.2013.02.035
20. Tăculescu E, Coricovac D, Soica C, Pinzaru I, Păcurariu C, Dehelean C. *Preclinical Aspects on Magnetic Iron Oxide Nanoparticles and Their Interventions as Anticancer Agents: Enucleation, Apoptosis and Other Mechanism*. IntechOpen; 2018.
21. Pisha E, Chai H, Lee S, et al. Discovery of betulinic acid as a selective inhibitor of human melanoma that functions by induction of apoptosis. *Nat Med*. 1995;1:1046–1051. doi:10.1038/nm1095-1046
22. Mullauer FB, Kessler JH, Medema JP. Betulinic acid, a natural compound with potent anticancer effects. *Anticancer Drugs*. 2010;21(3):215–227. doi:10.1097/CAD.0b013e3283357c62
23. Kumar P, Bhadauria AS, Singh AK, Saha S. Betulinic acid as apoptosis activator: molecular mechanisms, mathematical modeling and chemical modifications. *Life Sci*. 2018;209:24–33. doi:10.1016/j.lfs.2018.07.056

24. Saneja A, Arora D, Kumar R, Dubey RD, Panda AK, Gupta PN. Therapeutic applications of betulinic acid nanoformulations. *Ann N Y Acad Sci*. 2018;1421(1):5–18. doi:10.1111/nyas.13570
25. Soica C, Trandafirescu C, Danciu C, Muntean D, Dehelean C, Simu G. New improved drug delivery technologies for pentacyclic triterpenes: a review. *Protein Pept Lett*. 2014;21(11):1137–1145. doi:10.2174/0929866521666140807115109
26. Lorente C, Cabeza L, Clares B, et al. Formulation and in vitro evaluation of magnetoliposomes as a potential nanotool in colorectal cancer therapy. *Colloids Surf B Biointerfaces*. 2018;171:553–565. doi:10.1016/j.colsurfb.2018.07.070
27. Dadwal A, Baldi A, Kumar Narang R. Nanoparticles as carriers for drug delivery in cancer. *Artif Cells Nanomed Biotechnol*. 2018;46 (sup2):295–305. doi:10.1080/21691401.2018.1457039
28. Bixner O, Reimhult E. Controlled magnetosomes: embedding of magnetic nanoparticles into membranes of monodisperse lipid vesicles. *J Colloid Interface Sci*. 2016;466:62–71. doi:10.1016/j.jcis.2015.11.071
29. Rodrigues ARO, Mendes PMF, Silva PML, et al. Solid and aqueous magnetoliposomes as nanocarriers for a new potential drug active against breast cancer. *Colloids Surf B Biointerfaces*. 2017;158: 460–468. doi:10.1016/j.colsurfb.2017.07.015
30. Andhale VA, Patil PR, Dhas AU, Chauhan PD, Desai SV. Liposome: an emerging tool in drug carrier system. *J Pharm Tech*. 2016;8:10982–11011.
31. Wang X, Yang L, Chen ZG, Shin DM. Application of nanotechnology in cancer therapy and imaging. *CA Cancer J Clin*. 2008;58 (2):97–110. doi:10.3322/CA.2007.0003
32. Ianoş R, Tăculescu E, Păcurariu C, Lazău I, Joy P. Solution Combustion Synthesis and Characterization of Magnetite, Fe3O4, Nanopowders. *J Am Ceram Soc*. 2012;95:2236–2240. doi:10.1111/j.1551-2916.2012.05159.x
33. Sabate R, Barnadas-Rodriguez R, Callejas-Fernandez J, Hidalgo-Alvarez R, Estelrich J. Preparation and characterization of extruded magnetoliposomes. *Int J Pharm*. 2008;347(1–2):156–162. doi:10.1016/j.ijpharm.2007.06.047
34. Wildeboer R, Southern P, Pankhurst Q. On the reliable measurement of specific absorption rates and intrinsic loss parameters in magnetic hyperthermia materials. *J Phys D Appl Phys*. 2014;47:495003. doi:10.1088/0022-3727/47/49/495003
35. Iacob N, Schinteie G, Palade P, Ticos C, Kuncser V. Stepped heating procedure for experimental SAR evaluation of ferrofluids. *Eur Phys J E Soft Matter*. 2015;38:142. doi:10.1140/epje/i2015-15057-8
36. Skouras A, Papadia K, Mourtas S, Klepetsanis P, Antimisiaris SG. Multifunctional doxorubicin-loaded magnetoliposomes with active and magnetic targeting properties. *Eur J Pharm Sci*. 2018;123: 162–172. doi:10.1016/j.ejps.2018.07.044
37. Liu Y, Zhang X, Liu Z, et al. Gold nanoshell-based betulinic acid liposomes for synergistic chemo-photothermal therapy. *Nanomedicine*. 2017;13(6):1891–1900. doi:10.1016/j.nano.2017.03.012
38. Zhu L, Huo Z, Wang L, Tong X, Xiao Y, Ni K. Targeted delivery of methotrexate to skeletal muscular tissue by thermosensitive magnetoliposomes. *Int J Pharm*. 2009;370(1–2):136–143. doi:10.1016/j.ijpharm.2008.12.003
39. Poller JM, Zaloga J, Schreiber E, et al. Selection of potential iron oxide nanoparticles for breast cancer treatment based on in vitro cytotoxicity and cellular uptake. *Int J Nanomedicine*. 2017;12: 3207–3220. doi:10.2147/IJN.S132369
40. Volk J, Engelmann J, Leyhausen G, Geurtsen W. Effects of three resin monomers on the cellular glutathione concentration of cultured human gingival fibroblasts. *Dent Mater*. 2006;22(6):499–505. doi:10.1016/j.dental.2005.06.002
41. Kossatz S, Ludwig R, Dähring H, et al. High therapeutic efficiency of magnetic hyperthermia in xenograft models achieved with moderate temperature dosages in the tumor area. *Pharm Res*. 2014;31 (12):3274–3288. doi:10.1007/s11095-014-1417-0
42. Patil JR, Jayaprakasha GK, Murthy KNC, Tichy SE, Chetti MB, Patil BS. Apoptosis-mediated proliferation inhibition of human colon cancer cells by volatile principles of Citrus aurantifolia. *Food Chem*. 2009;114(4):1351–1358. doi:10.1016/j.foodchem.2008.11.033
43. Ghitu A, Schwiebs A, Radeke HH, et al. A comprehensive assessment of apigenin as an antiproliferative, proapoptotic, antiangiogenic and immunomodulatory phytocompound. *Nutrients*. 2019;11(4):858. doi:10.3390/nu11040858
44. Liang -C-C, Park AY, Guan J-L. In vitro scratch assay: a convenient and inexpensive method for analysis of cell migration in vitro. *Nat Protoc*. 2007;2(2):329–333. doi:10.1038/nprot.2007.30
45. Goetsch KP, Niesler CU. Optimization of the scratch assay for in vitro skeletal muscle wound healing analysis. *Anal Biochem*. 2011;411(1):158–160. doi:10.1016/j.ab.2010.12.012
46. Felice F, Zambito Y, Belardinelli E, Fabiano A, Santoni T, Di Stefano R. Effect of different chitosan derivatives on in vitro scratch wound assay: a comparative study. *Int J Biol Macromol*. 2015;76:236–241. doi:10.1016/j.ijbiomac.2015.02.041
47. Pavel IZ, Csuk R, Danciu C, et al. Assessment of the antiangiogenic and anti-inflammatory properties of a maslinic acid derivative and its potentiation using zinc chloride. *Int J Mol Sci*. 2019;20(11):2828. doi:10.3390/ijms20112828
48. Storgard C, Mikolon D, Stupack DG. Angiogenesis assays in the chick CAM. *Methods Mol Biol*. 2005;294:123–136. doi:10.1385/1-59259-860-9:123
49. Caunii A, Oprean C, Cristea M, et al. Effects of ursolic and oleanolic on SK-MEL-2 melanoma cells: in vitro and in vivo assays. *Int J Oncol*. 2017;51(6):1651–1660. doi:10.3892/ijo.2017.4160
50. Falamas A, Dehelean CA, Pinzaru SC. Monitoring of betulin nanoemulsion treatment and molecular changes in mouse skin cancer using surface enhanced Raman spectroscopy. *Vib Spectrosc*. 2018;95: 44–50. doi:10.1016/j.vibspec.2018.01.004
51. Pinzaru I, Coricovac D, Dehelean C, et al. Stable PEG-coated silver nanoparticles - a comprehensive toxicological profile. *Food Chem Toxicol*. 2018;111:546–556. doi:10.1016/j.fct.2017.11.051
52. Cinta Pinzaru S, Leopold N, Kiefer W. Vibrational spectroscopy of betulinic acid HIV inhibitor and of its birch bark natural source. *Talanta*. 2002;57(4):625–631. doi:10.1016/S0039-9140(02)00102-9
53. Khan S, Shah ZH, Riaz S, et al. Antimicrobial activity of citric acid functionalized iron oxide nanoparticles –Superparamagnetic effect. *Ceram Int*. 2020. doi:10.1016/j.ceramint.2020.01.109
54. Kawni I, Garcia R, Youssef S, Abboud M, Podlecki J, Habchi R. Stabilization and encapsulation of magnetite nanoparticles. *Mater Res Express*. 2016;3:125024. doi:10.1088/2053-1591/3/12/125024
55. Slavov L, Abrashev MV, Merodiiska T, et al. Raman spectroscopy investigation of magnetite nanoparticles in ferrofluids. *J Magn Magn Mater*. 2010;322(14):1904–1911. doi:10.1016/j.jmmm.2010.01.005
56. Testa-Anta M, Ramos-Docampo MA, Comesaña-Hermo M, Rivas-Murias B, Salgueiriño V. Raman spectroscopy to unravel the magnetic properties of iron oxide nanocrystals for bio-related applications. *Nanoscale Adv*. 2019;1(6):2086–2103. doi:10.1039/C9NA00064J
57. Franzé S, Selmin F, Samaritani E, Minghetti P, Cilurzo F. Lyophilization of liposomal formulations: still necessary, still challenging. *Pharmaceutics*. 2018;10(3):139. doi:10.3390/pharmaceutics10030139
58. Smith SM, Wunder MB, Norris DA, Shellman YG, Roemer K. A simple protocol for using a LDH-based cytotoxicity assay to assess the effects of death and growth inhibition at the same time. *PLoS One*. 2011;6(11):e26908. doi:10.1371/journal.pone.0026908
59. Weyermann J, Lochmann D, Zimmer A. A practical note on the use of cytotoxicity assays. *Int J Pharm*. 2005;288(2):369–376. doi:10.1016/j.ijpharm.2004.09.018
60. Estanqueiro M, Amaral MH, Conceicao J, Sousa Lobo JM. Nanotechnological carriers for cancer chemotherapy: the state of the art. *Colloids Surf B Biointerfaces*. 2015;126:631–648. doi:10.1016/j.colsurfb.2014.12.041

61. Wachsberger PR, Burd R, Wahl ML, Leeper DB. Betulinic acid sensitization of low pH adapted human melanoma cells to hyperthermia. *Int J Hyperth*. 2002;18(2):153–164. doi:10.1080/02656730110091333
62. Moaca E-A, Farcas C, Coricovac D, Loghin F, Dehelean C-A, Pacurariu C. Citric acid coated magnetic iron oxide nanoparticles (Fe3O4): synthesis, characterization and applications. In: The 5th Edition of Nanotech France 2019; International Conference and Exhibition; 2019; 157.
63. Ong SGM, Chitneni M, Lee KS, Ming LC, Yuen KH. Evaluation of extrusion technique for nanosizing liposomes. *Pharmaceutics*. 2016;8(4):36. doi:10.3390/pharmaceutics8040036
64. Faria MR, Cruz MM, Goncalves MC, Carvalho A, Feio G, Martins MBF. Synthesis and characterization of magnetoliposomes for MRI contrast enhancement. *Int J Pharm*. 2013;446(1–2):183–190. doi:10.1016/j.ijpharm.2013.02.025
65. Zhao T, Liu Y, Gao Z, et al. Self-assembly and cytotoxicity study of PEG-modified ursolic acid liposomes. *Mater Sci Eng C Mater Biol Appl*. 2015;53:196–203. doi:10.1016/j.msec.2015.04.022
66. Liu Y, Gao D, Zhang X, et al. Antitumor drug effect of betulinic acid mediated by polyethylene glycol modified liposomes. *Mater Sci Eng C Mater Biol Appl*. 2016;64:124–132. doi:10.1016/j.msec.2016.03.080
67. Allen TM, Cullis PR. Liposomal drug delivery systems: from concept to clinical applications. *Adv Drug Deliv Rev*. 2013;65(1):36–48. doi:10.1016/j.addr.2012.09.037
68. Kneidl B, Peller M, Winter G, Lindner LH, Hossann M. Thermosensitive liposomal drug delivery systems: state of the art review. *Int J Nanomedicine*. 2014;9:4387–4398. doi:10.2147/IJN.S49297
69. Kettering M, Winter J, Zeisberger M, et al. Magnetic nanoparticles as bimodal tools in magnetically induced labelling and magnetic heating of tumour cells: anin vitrostudy. *Nanotechnology*. 2007;18(17):175101. doi:10.1088/0957-4484/18/17/175101
70. Dutz S, Kettering M, Hilger I, Müller R, Zeisberger M. Magnetic multicore nanoparticles for hyperthermia-influence of particle immobilization in tumour tissue on magnetic properties. *Nanotechnology*. 2011;22:265102. doi:10.1088/0957-4484/22/26/265102
71. Laurent S, Dutz S, Hafeli UO, Mahmoudi M. Magnetic fluid hyperthermia: focus on superparamagnetic iron oxide nanoparticles. *Adv Colloid Interface Sci*. 2011;166(1–2):8–23. doi:10.1016/j.cis.2011.04.003
72. Putz A-M, Ianasi C, Dudas Z, et al. SiO2-PVA-Fe(acac)3 hybrid based superparamagnetic nanocomposites for nanomedicine: morpho-textural evaluation and in vitro cytotoxicity assay. *Molecules*. 2020;25(3):653. doi:10.3390/molecules25030653
73. Moaca E-A, Farcas C, Coricovac D, et al. Oleic acid double coated Fe(3)O(4) nanoparticles as anti-melanoma compounds with a complex mechanism of activity-in vitro and in ovo assessment. *J Biomed Nanotechnol*. 2019;15(5):893–909. doi:10.1166/jbn.2019.2726
74. Farcas CG, Macasoi I, Pinzaru I, et al. Controlled synthesis and characterization of micrometric single crystalline magnetite with superparamagnetic behavior and cytocompatibility/cytotoxicity assessments. *Front Pharmacol*. 2020;11:410. doi:10.3389/fphar.2020.00410
75. Soica C, Danciu C, Savoiu-Balint G, et al. Betulinic acid in complex with a gamma-cyclodextrin derivative decreases proliferation and in vivo tumor development of non-metastatic and metastatic B164A5 cells. *Int J Mol Sci*. 2014;15(5):8235–8255. doi:10.3390/ijms15058235
76. Soica C, Dehelean C, Danciu C, et al. Betulin complex in gamma-cyclodextrin derivatives: properties and antineoplastic activities in in vitro and in vivo tumor models. *Int J Mol Sci*. 2012;13(11):14992–15011. doi:10.3390/ijms131114992
77. Pilco-Ferreto N, Calaf G. Influence of doxorubicin on apoptosis and oxidative stress in breast cancer cell lines. *Int J Oncol*. 2016;49:753–762. doi:10.3892/ijo.2016.3558
78. Zheng Y, Liu P, Wang N, et al. Betulinic acid suppresses breast cancer metastasis by targeting GRP78-mediated glycolysis and ER stress apoptotic pathway. *Oxid Med Cell Longev*. 2019;2019:8781690. doi:10.1155/2019/8781690
79. Chaves NL, Estrela-Lopis I, Bottner J, et al. Exploring cellular uptake of iron oxide nanoparticles associated with rhodium citrate in breast cancer cells. *Int J Nanomedicine*. 2017;12:5511–5523. doi:10.2147/IJN.S141582
80. Lee YK, Choi E-J, Webster TJ, Kim S-H, Khang D. Effect of the protein corona on nanoparticles for modulating cytotoxicity and immunotoxicity. *Int J Nanomedicine*. 2015;10:97–113. doi:10.2147/IJN.S72998
81. Ferraro E, Pesaresi MG, De Zio D, et al. Apaf1 plays a pro-survival role by regulating centrosome morphology and function. *J Cell Sci*. 2011;124(20):3450–3463. doi:10.1242/jcs.086298
82. Field JJ, Kanakkanthara A, Miller JH. Microtubule-targeting agents are clinically successful due to both mitotic and interphase impairment of microtubule function. *Bioorg Med Chem*. 2014;22(18):5050–5059. doi:10.1016/j.bmc.2014.02.035
83. Madiraju C, Edler MC, Hamel E, et al. Tubulin assembly, taxoid site binding, and cellular effects of the microtubule-stabilizing agent dictyostatin. *Biochemistry*. 2005;44(45):15053–15063. doi:10.1021/bi050685l
84. Rohena CC, Risinger AL, Devambatla RKV, et al. Janus compounds, 5-chloro-N^4-methyl-N^4-aryl-9H-pyrimido[4,5-b]indole-2,4-diamines, cause both microtubule depolymerizing and stabilizing effects. *Molecules*. 2016;21(12):1661. doi:10.3390/molecules21121661
85. Fanale D, Bronte G, Passiglia F, et al. Stabilizing versus destabilizing the microtubules: a double-edge sword for an effective cancer treatment option? *Anal Cell Pathol (Amst)*. 2015;2015:690916. doi:10.1155/2015/690916
86. Buey RM, Barasoain I, Jackson E, et al. Microtubule interactions with chemically diverse stabilizing agents: thermodynamics of binding to the paclitaxel site predicts cytotoxicity. *Chem Biol*. 2005;12(12):1269–1279. doi:10.1016/j.chembiol.2005.09.010
87. Lu S-J, Feng Q, Park JS, et al. Biologic properties and enucleation of red blood cells from human embryonic stem cells. *Blood*. 2008;112(12):4475–4484. doi:10.1182/blood-2008-05-157198
88. Prescott DM, Myerson D, Wallace J. Enucleation of mammalian cells with cytochalasin B. *Exp Cell Res*. 1972;71(2):480–485. doi:10.1016/0014-4827(72)90322-9
89. Paunescu V, Bojin FM, Gavriliuc OI, et al. Enucleation: a possible mechanism of cancer cell death. *J Cell Mol Med*. 2014;18(6):962–965. doi:10.1111/jcmm.12271
90. Dehelean CA, Feflea S, Ganta S, Amiji M. Anti-angiogenic effects of betulinic acid administered in nanoemulsion formulation using chorioallantoic membrane assay. *J Biomed Nanotechnol*. 2011;7(2):317–324. doi:10.1166/jbn.2011.1297
91. Ribatti D. The chick embryo chorioallantoic membrane (CAM). A multifaceted experimental model. *Mech Dev*. 2016;141:70–77. doi:10.1016/j.mod.2016.05.003
92. Nik ME, Malaekeh-Nikouei B, Amin M, et al. Liposomal formulation of Galbanic acid improved therapeutic efficacy of pegylated liposomal Doxorubicin in mouse colon carcinoma. *Sci Rep*. 2019;9(1):9527. doi:10.1038/s41598-019-45974-7
93. Ribatti D, Nico B, Ruggieri S, Tamma R, Simone G, Mangia A. Angiogenesis and antiangiogenesis in triple-negative breast cancer. *Transl Oncol*. 2016;9(5):453–457. doi:10.1016/j.tranon.2016.07.002
94. Farcas CG, Moaca EA, Dragoi R, et al. Preliminary results of betulinic acid-loaded magnetoliposomes - A potential approach to increase therapeutic efficacy in melanoma. *Rev Chim*. 2019;70(9):3372–3377. doi:10.37358/rc.19.9.7552
95. Farcas C, Tăculescu E, Coricovac D, Dehelean C, Loghin F. In vitro antiproliferative effects of Fe3O4_BA loaded liposomes. *Toxicol Lett*. 2018;295:S113. doi:10.1016/j.toxlet.2018.06.646